Maxwell-Wagner-Sillars interfacial polarization in dielectric spectra of composite materials: Scaling laws and applications

Mariem Samet, Ali Kallel, Anatoli Serghei

Maxwell-Wagner-Sillars interfacial polarization in dielectric spectra of composite materials: Scaling laws and applications

Mariem SAMET[1,2], Ali KALLEL[2], Anatoli SERGHEI[1]

[1]*Université Claude Bernard Lyon1, Ingénierie des Matériaux Polymères, CNRS UMR 5223, Villeurbanne, France*
[2]*Faculté des Sciences de Sfax, Laboratoire des Matériaux Composites Céramiques et Polymères, 3018 Sfax, Tunisie*

ABSTRACT

An experimental and theoretical investigation of the scaling laws governing the phenomenon of Maxwell-Wagner-Sillars interfacial polarization in composite materials in dependence on morphology, volume fraction, orientation of fillers, form factor and presence of interphases is presented in the current study. By considering the complex dielectric function of the matrix and of the fillers, the dielectric spectra are calculated in the frequency range from 10^7 Hz to 10^{-2} Hz and compared to dielectric measurements by Broadband Dielectric Spectroscopy, carried out in the frequency range from 10^7 Hz to 0.5 Hz and between -90 ^{o}C and 150 ^{o}C. The characteristic frequencies of the global dielectric response are reported to strongly vary with the conductivity value of the conductive phase, while a much weaker dependence is observed upon varying the volume fraction, the form factor and the orientation of fillers. The value of permittivity at low frequency does not change with the conductivity value, whereas a significant variation is observed in dependence on the composite morphology, form factor, orientation of fillers and presence of interfaces with different gradients of properties. Two possible applications of our analysis are reported: (i) measuring the conductivity of materials without employing a direct electrical contact between the electrodes and the sample and (ii) discriminating different phenomena of electrical polarization in complex materials by analyzing the scaling laws. Our study delivers thus a useful and necessary analysis of the dielectric behavior of composite materials, where interfacial polarization effects play a major role.

Corresponding author: mariem.samet@gmail.com

1. Introduction

The electrical and dielectric properties of homogeneous materials can be fully described by the complex dielectric permittivity function $\varepsilon^* = \varepsilon' - i\varepsilon''$ (or by the complex conductivity function $\sigma^* = \sigma' + i\sigma''$, with $\sigma^* = i\omega\varepsilon_0\varepsilon^*$)[1]. The spectral and temperature dependence of ε^* directly reveal phenomena taking place at the molecular scale such as dipolar relaxation processes[2-4], phase transitions[5-7] and charge transport processes[8-13]. The direct correlation existing between the spectral dependence of ε^* and molecular phenomena is drastically impacted by the presence of interfaces and interphases, when the materials under study are heterogeneous (composite materials, multiphase materials, etc.). From an electrical point of view, an interface is an internal surface between two phases having different electrical and dielectric properties[14]. The existence of internal surfaces separating two different dielectric phases (phase A and phase B) has a major consequence on the interpretation of the dielectric properties of heterogeneous materials[15-23]. The global dielectric response must be described in this case by two different complex dielectric functions: the complex dielectric permittivity function of the phase A ($\varepsilon_A^* = \varepsilon_A' - i\varepsilon_A''$) and the complex dielectric permittivity function of the phase B $\left(\varepsilon_B^* = \varepsilon_B' - i\varepsilon_B''\right)$. If an interphase is formed between the two phases, a third complex dielectric function must be taken into account to describe the dielectric behavior of the system under study ($\varepsilon_{interphase}^* = \varepsilon'_{interphase} - i\varepsilon''_{interphase}$). The global dielectric response in such systems becomes thus a complicated average of ε_A^* and ε_B^* (eventually, also, of $\varepsilon_{interphase}^*$), not anymore reflecting only molecular phenomena taking place in phase A or phase B, but also giving rise to new phenomena appearing in the dielectric spectra of heterogeneous materials. For instance, the phenomenon of interfacial polarization gives rise to the appearance of new dielectric features resembling molecular relaxation phenomena but to which they do not have any direct physical correspondence. Furthermore, the presence of interfacial polarization can distort the dielectric spectra of molecular relaxation processes, causing apparent shifts in their frequency position and broadening effects[6]. As opposed to the homogenous material described by only one complex dielectric function, the direct molecular assignment of a

dielectric spectrum is thus generally lost in a heterogeneous material and a detailed analysis employing two or more complex dielectric functions must be carried-out in order to describe its spectral behavior.

The aim of the present study is to thoroughly analyze the electrical and dielectric properties of composites materials in systematic dependence on morphology, volume fraction, orientation of fillers, form factor and presence of interphases exhibiting different gradients of local properties. In the scientific literature, the global dielectric response of heterogeneous materials is usually treated using dielectric mixing models using effective medium approaches[24-40]. These models give precise determinations of mean dielectric parameters, but without a systematic analysis of the scaling laws governing the characteristic frequencies in a broad frequency range. In the present study, the characteristic frequencies defining the global dielectric response of composite materials are thoroughly investigated and their scaling laws are analyzed in a broad frequency range. Our study delivers a useful and necessary analysis of the dielectric behavior of composite materials, where interfacial polarization effects play a major role.

2. Methods and Materials:

Methods: The dielectric measurements were carried-out using a high resolution dielectric spectrometer (Alpha Analyzer) from Novocontrol GmbH, assisted by a Quatro Temperature Controller. The samples have been measured in a parallel-plate geometry using brass electrodes. The applied voltage was 0.1 V. The temperature was controlled under flow of pure nitrogen gas, leading to stabilization conditions better than 0.1 ^{o}C for the absolute temperature.

Materials: Two polymeric materials have been investigated: poly(vinyl acetare) (**PVAc**, Mw = 100.000 g/mol, density= 1.19 g/cm^{-3}, purchased from Sigma Aldrich) and poly(2-vynil-pyridine) (**P2VP**, Mw = 37.500 g/mol, density=0.97 g/cm^{-3}, purchased from Sigma Aldrich). The samples were prepared in form of films of 100 μm in thickness.

3. The phenomenon of interfacial polarization

The basic principle of the phenomenon of interfacial polarization is related to the contrast in the dielectric loss (or in the conductivity value) taking place across an internal interface that separates local different dielectric phases of a composite material. The orientation of the internal interface in respect to the direction of the applied electric field is of crucial importance. In order to exemplify the basic principle of this phenomenon, the simplest experimental situation is considered in Figure 1: two layers exhibiting a contrast in their dielectric loss and measured by applying an electric field perpendicularly to their surfaces. In order to experimentally realize these conditions, two fully amorphous polymers exhibiting a large difference in their glass transition temperature have been chosen: poly(vinyl acetare) (PVAc, with a glass transition temperature of Tg(PVAc)= 40^0C) and poly(2-vynil-pyridine) (P2VP, with a glass transition temperature of Tg(P2VP)= 155^0C). To simplify the experimental conditions even more, a metal electrode has been placed between the two layers, in order to completely eliminate the possibility of the interphase that could be formed at the contact between the two polymer phases. This corresponds to a measured global dielectric response originating from to two dielectric contributions: the contribution of the bulk PVAc and the contribution of the bulk P2VP. When an interphase is formed between the two phases (not the case for the data presented in Figure 1), a third dielectric contribution, that of the interphase, must be comprised in the global dielectric response. In the case presented in Figure 1, the measured dielectric response is thus given by:

$$\frac{1}{C^*_{meas}} = \frac{1}{C^*_{PVAc}} + \frac{1}{C^*_{P2VP}} \qquad \text{(eq.1)}$$

Where: $C^*_{meas} = C'_{meas} + iC''_{meas}$ represents the measured complex capacity, $C^*_{PVAc} = C'_{PVAc} + iC''_{PVAc}$ the complex capacity of the PVAc layer and $C^*_{P2VP} = C'_{P2VP} + iC''_{P2VP}$ the complex capacity of the P2VP layer. Eq. 1 corresponds to a serial circuit of two complex capacities (or, since $Z^* = \frac{1}{\left(i\omega C^*\right)'}$ of two complex impedances) and it can be equivalently expressed as:

$$Z^*_{meas} = Z^*_{PVAc} + Z^*_{P2VP} \quad \text{(eq.2)}$$

Where: Z^*_{meas} represents the measured complex impedance, Z^*_{PVAc} the complex impedance of the PVAc layer and Z^*_{P2VP} the complex capacity of the P2VP layer.

Based on the complex capacity C^*, representing the measurable parameter in a dielectric experiment, the complex dielectric permittivity $\varepsilon^* = \varepsilon' - i\varepsilon''$ of the material under study can be determined using the following relation:

$$C^* = \varepsilon_0 \varepsilon^* \frac{A}{d} \quad \text{(eq.3)}$$

Where: $\varepsilon_0 = 8.854 \times 10^{-12} \frac{Vm}{As}$ represents the vacuum permittivity, d the sample thickness and A the surface area of the sample. Eq. 1 can be thus re-written as:

$$\frac{d_{sample}}{\varepsilon^*_{meas}} = \frac{d_{PVAc}}{\varepsilon^*_{PVAc}} + \frac{d_{P2VP}}{\varepsilon^*_{P2VP}} \quad \text{(eq.4)}$$

Where: $\varepsilon^*_{meas} = \varepsilon'_{meas} - i\varepsilon''_{meas}$ represents the measured complex dielectric permittivity, $\varepsilon^*_{PVAc} = \varepsilon'_{PVAc} - i\varepsilon''_{PVAc}$ the complex permittivity of the PVAc layer, $\varepsilon^*_{P2VP} = \varepsilon'_{P2VP} - i\varepsilon''_{P2VP}$ the complex permittivity of the P2VP layer and d_{sample}, d_{PVAc} and d_{P2VP} the total sample thickness and the thickness of the PVAc and P2VP layer, respectively.

The dielectric loss ε''_{PVAc} of the bulk PVAc and the dielectric loss ε''_{P2VP} of the bulk P2VP are presented in Figure 1a, b, d, e as a function of temperature at a fixed frequency (100 Hz) and as a function of frequency at a fixed temperature (120°C). For PVAc, a relaxation peak related to the dynamic glass transition (alpha relaxation) is observed around 60°C (Figure 1a). The alpha relaxation peak is followed, at higher temperatures, by the conductivity contribution. For P2VP, the alpha relaxation peak is observed around 125°C (Figure 1b). When PVAc and P2VP are measured together in bi-layer morphology (Figure 1c), the global dielectric response, given by eq. 1, shows three peaks in the dielectric loss: a peak corresponding to the alpha relaxation of PVAc, a peak corresponding to the alpha relaxation of P2VP and a third peak, appearing around 85^0C, whose origin is related to the

phenomenon of MWS interfacial polarization (Figure 1c). A similar behavior is found by looking at the experimental data of the dielectric loss as a function of frequency (Figure 1 d, e, f). Between the alpha relaxation peak of PVAc appearing slightly above 10^6 Hz (Figure 1d) and the alpha relaxation peak of P2VP observed slightly below 10^2 Hz, a third peak is detected around 10^4 Hz, when the PVAc and the P2VP layers are measured together in a bi-layer structure (Figure 1 f). This peak is the same peak detected around 60°C in the dielectric spectrum shown as a function of temperature (Figure 1c) and it is thus related the phenomenon of interfacial polarization. This MWS contribution, appearing frequently in dielectric spectra of multiphase materials (composite materials, heterogeneous materials, etc.), arises basically from a contrast in the dielectric loss (or in the conductivity) taking place across the internal interface separating the two different dielectric phases. We note that, according to Figure1, neither the formation of an interphase nor a physical contact between the dielectric phases is a necessary condition for the appearance of the interfacial polarization. The three dielectric peaks observed in Figure 1c represent thus the measured average of the spectra presented in Figure 1a and Figure 1b, according to the equation 1. In the same way, the dielectric data measured in Figure 1f represent the measured average of the spectra presented in Figure 1d and Figure 1e, according to the same equation 1. Additional experimental data, measured at different frequencies and at different temperatures, are presented in the Supplementary Material (Figure S1 and S2).

For a deeper understanding of this phenomenon, the voltage distribution across a multiphase material is analyzed in Figure 2, by considering the simplest morphology represented by a two-layer structure. On this structure, a total voltage of V_T=1 V is applied at different frequencies between 10^7 Hz and 10^{-2} Hz. For the sake of simplicity, we shall consider in our calculations two dielectric phases (phase A and phase B) having an identical permittivity value $(\varepsilon_A = \varepsilon_B = 3)$, an identical thickness $(d_A = d_B = 0.1mm)$ and showing a difference of 3 orders of magnitude between their dielectric losses. This difference of 3 decades in the dielectric losses (corresponding roughly to the contrast shown on Figure 1 between PVAc and P2VP) is related in our calculations to a difference of 3 decades in the conductivity values of the two phases (conductivity of phase A: $\sigma_A = 10^{-8} S/cm$, conductivity

of phase B: $\sigma_B = 10^{-11} S/cm$). In the global response of the two phases, a peak in the dielectric loss is observed at a characteristic frequency of 3 x 10^3 Hz, related to the phenomenon of MWS interfacial polarization. At high frequencies, well above the characteristic frequency of the MWS peak, the total voltage V_T=1V applied on the bi-layer structure is distributed between the two dielectric phases A and B. In our particular case, the voltages across phase A and B are equal (V_A=V_B=0.5 V), because of the fact that the two phases have identical permittivity values and identical thicknesses. More generally, it can be easily shown that, at high frequencies, the voltage distribution between the two phases is actually governed by the values of permittivity and thickness (see Figure S3 from Supplementary Information). At low frequencies, below the characteristic frequency of the MWS peak, the voltage applied on the bi-layer structure falls entirely on the phase B. Thus V_T=V_B=1 V, while V_A=0 V. This is due to the fact that, at high frequencies, the measured impedance comprises contributions from both phases A and B, while at low frequencies only the impedance of the phase B is measured. As shown in Figure 2, the characteristic frequency of the MWS peak marks thus the transition between a measurement reflecting the phase A and phase B to a measurement reflecting only the phase B. This is experimentally validated in Figure 3, where the measured impedance values corresponding to the experimental data presented in Figure 1 are shown. At high frequencies, both PVAc and P2VP contribute to the total impedance measurement, but, as the frequency decreases below the characteristic value of f_{MWS}, the measurement reflects only the impedance of P2VP. This is because, in this frequency range, the impedance of PVAc is by orders of magnitude lower than that of P2VP, being practically negligible. In the same time, while only the impedance of P2VP contributes the total measurement, the effective parameters are still calculated from the measured impedance using the total thickness of sample, which is the sum of the thicknesses of both PVAc and P2VP. This is the reason why, as shown in Figure 2, two dielectric phases of equal permittivity values ($\varepsilon_A = \varepsilon_B = 3$) give rise, in the frequency range lower than the characteristic frequency f_{MWS}, to an effective permittivity of 6.

In conclusion, the MWS interfacial polarization is an important phenomenon appearing in multiphase materials (composite materials, heterogeneous materials, etc.),

leading to a voltage distribution across the local dielectric phases that changes with the frequency of the applied electric field. As a direct consequence, this phenomenon gives rise to dielectric dispersions appearing as peaks in the spectra of dielectric loss. Thus, for understanding the dielectric behavior of multiphase materials, the scaling laws of this phenomenon have to be systematically analyzed in dependence on the conductivity value, frequency, volume fraction of the local dielectric phases, morphology, orientation, form factor, presence of interphases showing gradients of local properties etc. This is analysis is carried-out in the following section.

4. Theoretical analysis

The global dielectric behavior of a two-phase composite material can be calculated as a function of the morphology using the following formulas (more details are provided in Supplementary Information):

(1) for a bi-layer morphology (when the electric field is perpendicular to the surface of the layers):

$$\varepsilon_{net}^{*} = \frac{\varepsilon_1^{*}\varepsilon_2^{*}}{\Phi\varepsilon_1^{*} + (1-\Phi)\varepsilon_2^{*}} \qquad \text{(eq.5)}$$

Where: ε_1^* and ε_2^* are the complex dielectric functions of the two phases and $\Phi = d_{ins}/L$ being the volume fraction of the insulating phase. The case when the applied electric field is parallel to the surface of the layers is trivial: the global response is a linear combination of ε_1^* and ε_2^* and the presence of the interface has no impact on the dielectric spectra (unless an interfacial layer is formed between the two phases, in which case a third dielectric function has to be taken into account).

(2) for a spherical morphology, the Maxwell- Garnett[41-43] equation can be used:

$$\varepsilon_{net}^{*} = \frac{\varepsilon_{matrix}^{*}\left[\varepsilon_{filler}^{*}(1+2\Phi) + 2\varepsilon_{matrix}^{*}(1-\Phi)\right]}{\left[\varepsilon_{filler}^{*}(1-\Phi) + \varepsilon_{matrix}^{*}(2+\Phi)\right]} \qquad \text{(eq.6)}$$

Where: ε^*_{matrix} represents the complex dielectric permittivity function of the matrix, ε^*_{filler} the complex dielectric permittivity of the fillers (or of the domains) and Φ the volume fraction of the fillers.

(3) for a cylindrical morphology[44]:

$$\varepsilon^*_{net} = \varepsilon^*_{marix}\left[1+2\Phi\frac{\varepsilon^*_{filler}-\varepsilon^*_{matrix}}{\varepsilon^*_{matrix}+\varepsilon^*_{filler}}\right] \quad \text{(eq.7)}$$

(4) for a ellipsoidal morphology, the following formula has been derived in previous studies[44-47]:

$$\varepsilon^*_{net} = \varepsilon^*_{matrix}\left[1+\Phi\sum_{k=x,y,z}\frac{\varepsilon^*_{filler}-\varepsilon^*_{matrix}}{\varepsilon^*_{matrix}+\left(\varepsilon^*_{filler}-\varepsilon^*_{matrix}\right)L_k}\cos^2\varphi_k\right] \quad \text{(eq.8)}$$

Where: $\Phi = 4\pi R_x R_y R_z N/3$ represents the volume fraction of the ellipsoidal filler (or domains), N is the number of particles per unit volume, and L_k is the depolarization factor along the k-axis, with $L_x+L_y+L_z=1$.

In the case of ellipsoidal fillers, another important parameter to be considered is related to the impact of orientation effects. Thus, the dielectric response of composite materials with randomly oriented ellipsoidal fillers is given by:

$$\varepsilon^*_{net} = \varepsilon^*_{matrix}\left[1+\frac{1}{3}\Phi\sum_{k=x,y,z}\frac{\varepsilon^*_{filler}-\varepsilon^*_{matrix}}{\varepsilon^*_{matrix}+\left(\varepsilon^*_{filler}-\varepsilon^*_{matrix}\right)L_k}\right] \quad \text{(eq.9)}$$

With: $\left\langle\cos^2\varphi_k\right\rangle = 1/3$

In the case of oriented fillers, the formula becomes:

$$\varepsilon^*_{net} = \varepsilon^*_{matrix}\left[1+\Phi\frac{\varepsilon^*_{filler}-\varepsilon^*_{matrix}}{\varepsilon^*_{matrix}+\left(\varepsilon^*_{filler}-\varepsilon^*_{matrix}\right)L_k}\right] \quad \text{(eq.10)}$$

Where: the factor L_k reflects the orientation of the fillers in respect to the direction of the applied electric field. Thus, for ellipsoids with the long axis oriented parallel with the direction of the applied electric field:

$$L_z = -\frac{1}{q^2-1} + \frac{q}{(q^2-1)^{3/2}} ln\left[q + (q^2-1)^{1/2}\right] \quad \text{(eq.11a)}$$

$$L_x = L_y = (1 - L_z)/2 \quad \text{(eq.11b)}$$

While for a perpendicular orientation between the long axis of the fillers and the direction of the applied electric field:

$$L_z = \frac{1}{1-q^2} - \frac{q}{(1-q^2)^{3/2}} cos^{-1} q \quad \text{(eq.11c)}$$

$$L_x = L_y = (1 - L_z)/2 \quad \text{(eq.11d)}$$

The above formula will be used in the following to perform numerical calculations of the global dielectric response of composite materials in dependence on conductivity, frequency, volume fraction of the local dielectric phases, morphology, orientation, form factor and presence of interphases with gradients of local properties.

4.1 The influence of morphology

Different morphologies of a two-phase composite material are taken into account (layered, spherical, cylindrical and ellipsoidal), while keeping constant all the other parameters that play a role for the phenomenon of interfacial polarization. For the cylindrical and the ellipsoidal morphology, a random orientation of fillers is considered. The results are presented in Figure 4. At high frequencies, the global dielectric response gives a dielectric permittivity that is identical to the permittivity values of the two phases (supposed equal, for the sake of simplicity). As we decrease the frequency; the phenomenon of MWS interfacial polarization starts to play an important role. It is manifested by a peak in the dielectric loss, marking the transition to much lower values of conductivity (corresponding to the phase which is less conductive). In the same time, an increase in the values of the net permittivity is observed, which is typical for the phenomenon of interfacial polarization. At constant values of ε_m^* and ε_f^* and at a constant value of the volume fraction

(taken 20% in the shown calculations), the position of the MWS peak and the plateau values of ε' at low frequencies change with the morphology. The highest value of ε' is observed for the ellipsoidal morphology while the lowest one for the layered morphology. In the following sections the scaling laws of the characteristic frequencies defining the global dielectric response will be analysed, for each morphology, in dependence on the conductivity, volume fraction, orientation of fillers, form factor and presence of interphases with different gradients of local properties.

In order to analyze the scaling laws, several characteristic frequencies are defined, as follows (Figure 5):

(a) f_{on} represents the onset of interfacial polarization effects, it is the frequency where the net permittivity value starts to increase with decreasing frequency, due to interfacial polarization effects.

(b) f_i is the inflexion point where the first derivative of the net permittivity in respect to frequency shows a maximum and where the second derivative is equal to zero.

(c) f_{MWS} is the frequency position of the MWS interfacial polarization peak observed in the net dielectric loss.

(d) f_{max}, is the frequency where the increase in the net permittivity starts to show a "saturation" plateau value in the low frequency region of the dielectric spectra.

4.2 The influence of conductivity

The influence of the variation of the conductivity of fillers (or domains) is taken into account, for three different morphologies, by keeping constant the complex permittivity function of the matrix and the volume fraction. For the ellipsoidal morphology, a random orientation of fillers is considered. The results are presented in Figure 6. As expected, all the characteristic frequencies are shifted to higher values with increasing the conductivity. No change in the plateau value of ε'_{net} at low frequencies is observed upon varying the conductivity. A detailed quantitative analysis is presented in Figure 7. The following scaling laws can be readily derived:

$f_{max} \sim f_i \sim f_{on} \sim f_{MWS} \sim \sigma_{DC}$ (eq.12)

$f_i^2 = f_{on} f_{max}$ (eq.13)

And σ_{DC} is defined as the plateau observed in frequency dependence of σ'.

4.3 The influence of volume fraction

The influence of the variation of the volume fraction is taken into account, for three different morphologies, by keeping constant the complex permittivity function of the matrix and of the fillers (or of the domains). The results are presented in Figure 8. As expected, the plateau value of the dielectric permittivity varies with the variation of the volume fraction. In the same time, only a little variation is observed for the position of the MWS interfacial polarization peak. A quantitative analysis is presented in Figure 9. One can deduce that $f_i^2 = f_{on} f_{max,}$ which is identical to the scaling law expressed by the eq. 13 upon varying the value of conductivity.

4.4 The influence of orientation of fillers

The influence of the orientation of fillers is taken into account for an ellipsoidal morphology, by keeping constant the complex permittivity function of the matrix and of the fillers (or of the domains) and the value of the volume fraction. Three different orientations are considered: random and parallel and perpendicular to the direction of the applied electric field. The results are presented in Figure 10. As expected, it is observed that the plateau value of ε'_{net} in the low frequency range strongly depends on the orientation. The highest value is obtained for the parallel orientation, while the lowest one for the perpendicular one. In the same time, less obvious, the frequency position of the MWS interfacial polarization changes as well. A systematic analysis upon varying the conductivity (while keeping a constant volume fraction) and the volume fraction (while keeping constant the conductivity value) is shown in Figure 11, for three different

orientations (random, parallel and perpendicular). A detailed quantitative analysis of the characteristic frequencies is shown in Figure 12.

It is thus observed that $f_{max} \sim f_i \sim f_{on} \sim f_{MWS} \sim \sigma_{DC}$ and $f_i^2 = f_{on} f_{max}$, which are identical to the scaling laws derived before. It is equally observed that the characteristic frequencies show a negligible dependence on the volume fraction of the fillers (or of domains). The quantitative analysis of the plateau values of ε'_{net} in the low frequency range presented in Figure 13 reveals a linear dependence in respect to the variation of the volume fraction. The most pronounced changes are observed for the parallel orientation of fillers.

4.5 The influence of the form factor

The influence of the form factor is taken into account by varying the form factor of ellipsoidal fillers and keeping constant all the other parameters that play a role (the complex dielectric function of the two phases, the volume fraction, the orientation). The results are shown in Figure 14. It is observed that the plateau value of ε'_{net} in the low frequency range strongly depends on the form factor of ellipsoidal fillers and that the frequency position of the MWS interfacial polarization changes as well. With increasing the form factor, the values of ε'_{net} increase and the MWS peak is shifted to lower frequencies (Figure 15). Parallel dependencies are observed, implying:

$$f_{max} \sim f_i \sim f_{on} \sim f_{MWS}. \qquad \text{(eq.14)}$$

which is identical with the scaling laws that were determined before.

4.6 The influence of the presence of interphases with different gradients of properties

When an interphase is formed between two phases A and B (characterized by $\varepsilon_A^* = \varepsilon'_A - i\varepsilon''_A$ and $\varepsilon_B^* = \varepsilon'_B - i\varepsilon''_B$), a third complex dielectric function, that of the interphase, must be taken into account for modeling the global dielectric behavior of the system. For

the sake of simplicity, this analysis is carried out in the present section for the case of a layered morphology.

For a material consisting of two layers (A of thickness d_A and B of thickness d_B), the net complex dielectric permittivity when the electric field is perpendicular to the surface of the layers can be written as:

$$\frac{d_A + d_B}{\varepsilon^*_{net}} = \frac{d_A}{\varepsilon^*_A} + \frac{d_B}{\varepsilon^*_B} \qquad \text{(eq.15)}$$

If an interphase of thickness d_i is formed between the phases A and B, the complex dielectric function of the interphase $\varepsilon^*_{interphase} = \varepsilon'_{interphase} - i\varepsilon''_{interphase}$ must be included in the calculations. Generally, the local dielectric properties in the interphase show a gradual variation depending on the local coordinate x between the two phases A and B, thus $\varepsilon'_{interphase} = \varepsilon'_{interphase}(x)$ and $\varepsilon''_{interphase} = \varepsilon''_{interphase}(x)$. In this case, the previous formula must be replaced by:

$$\frac{d_A + d_i + d_B}{\varepsilon^*_{net}} = \frac{d_A}{\varepsilon^*_A} + \int_0^{di} \frac{dx}{\varepsilon'_{\text{interphase}}(x) - i\varepsilon'_{\text{interphase}}(x)} + \frac{d_B}{\varepsilon^*_B} \qquad \text{(eq.16)}$$

The above formula is applied in the following in order to emphasize the impact of the presence of interphases with different gradients of local properties. Four situations are compared:

(a) No interphase is formed; the system is described by two complex dielectric functions, according to the eq. 15.

(b) An interphase is formed, having constant local properties. The system is described by:

$$\frac{d_A + d_i + d_B}{\varepsilon^*_{net}} = \frac{d_A}{\varepsilon^*_A} + \frac{d_i}{\varepsilon^*_{\text{interphase}}} + \frac{d_B}{\varepsilon^*_B} \qquad \text{(eq.17)}$$

(c) An interphase is formed, with a linear gradient of local properties between phase A and phase B. The effective dielectric function of the interphase can be calculated by solving the integral shown in eq. 16, which leads to:

$$\frac{1}{\varepsilon^*_{eff}} = \left[\frac{-i * Log\left(\varepsilon' + i\left(\frac{\varepsilon''_{cond} - \varepsilon''}{L} x + \varepsilon''_{ins} \right) \right)}{\varepsilon''_{cond} - \varepsilon''_{ins}} \right]_0^L \qquad \text{(eq.18)}$$

With: L being the thickness of the interphase, ε''_{cond} the dielectric loss of the phase which is more conductive and ε''_{ins} the dielectric loss of the phase which is less conductive.

(d) An interphase is formed, with an exponential gradient of local properties between phase A and phase B. The effective dielectric function of the interphase can be calculated by solving the integral shown in (eq.16), leading to:

$$\frac{1}{\varepsilon^*_{eff}} = \left[\frac{-L * Log\left(\varepsilon' + \varepsilon''^2_{ins} \left(\varepsilon''_{cond} / \varepsilon''_{ins} \right)^{\frac{2x}{L}} \right)}{2\varepsilon' \log\left(\varepsilon''_{cond} / \varepsilon''_{ins} \right)} - \frac{-i * L * Log\left(\frac{\varepsilon''_{ins} \left(\varepsilon''_{cond} / \varepsilon''_{ins} \right)^{\frac{x}{L}}}{\varepsilon'} \right)}{\varepsilon' \log\left(\varepsilon''_{cond} / \varepsilon''_{ins} \right)} + \frac{x}{\varepsilon'} \right]_0^L \qquad \text{(eq.19)}$$

Numerical calculations according to the four situations presented above are shown in Figure 16. While a detailed analysis is out of the scope of the present section, several obvious conclusions can be drawn:

(a) First of all, in the limit of high frequencies (above 1 MHz for the case presented in Figure 16), no impact of the presence of interfaces or interphases is observed, all dielectric curves coincide.

(b) Secondly, a significant difference in the global dielectric behavior is observed when an interphase is present at the interface between two different dielectric phases.

(c) Thirdly, the impact of the presence of an interphase strongly depends on the form of the gradient of the local dielectric properties between the two phases.

For a deeper analysis of the impact of interphases, further analytical and numerical approaches are required. While taking into consideration effects of interphases remains still a relatively simple mathematical problem when constant local properties are assumed, analyzing more realistic profiles exhibiting gradients of local properties can become very rapidly complicated to solve, especially when less simple morphologies are considered (as for instance, spherical or ellipsoidal). The scope of the present section of our study was to demonstrate the first steps of a rigorous analytical approach that allows one to analyze the impact of interphases in dependence on the profile of their gradient of local properties.

5. Experimental investigations of interfacial polarization effects

The most important difficulty in experimentally analyzing the scaling laws of the phenomenon of interfacial polarization in multi-phase materials is related to the non-ideal distribution of properties specific to composite materials. The fillers are often not uniformly distributed in the volume of the matrix and quite frequently aggregation phenomena are observed. Furthermore, for composite materials prepared by solvent casting, sedimentation effects can be observed when a significant difference in density exists between the fillers and the matrix. Moreover, even for very low volume fractions, percolation phenomena can take place when fillers with a high form factor are employed. Not at last, the fillers do not have constant dimensions characterizing their shape but they show a distribution of sizes around an average value. An ideal composite material is therefore difficult to realize experimentally. Therefore, since aggregation effects, sedimentation effects, percolation effects and fillers with a non-uniform size distribution are not analyzed in the present study, only two morphologies could be chosen to experimentally exemplify the scaling laws of multiphase materials: a bi-layer morphology and a cylindrical morphology. Both morphologies were at the macroscopic scale, offering thus the experimental control needed

to approach the ideal situations analyzed by our numerical simulations. The experimental data and their analysis are presented in the Supplementary Information.

5. Applications

5.1 Discrimination of different electrical polarization phenomena

Two different forms of the phenomenon of electrical polarization, namely the interfacial polarization in bi-layer materials and the electrode polarization in ion-conducting materials, can be analyzed using an identical equation (eq. 15). This is because, in both cases, the global dielectric response is given by a serial circuit of two complex capacities, where two different dielectric function must be taken into consideration: (a) the dielectric functions of the two different dielectric phases, in the case of interfacial polarization; (b) the dielectric function of the bulk and that of the interfacial layers formed in contact with the measurement electrodes in the case of electrode polarization[6,13,14,48-50]. Both situations lead to dielectric curves having a similar shape (Figure 17), both showing a dielectric peak in the global dielectric loss. However, despite the fact that both phenomena of electrical polarization can de described by using the same mathematical formalism (eq. 15), a detailed analysis of the characteristic frequencies in dependence on the volume fraction Φ of the less conductive phase (of the interfacial layers in the case of electrode polarization) lead surprisingly to a fundamental difference: while the frequency position of the dielectric peak appears precisely at the inflexion point given by f_i in the case of interfacial polarization, the dielectric peak appears at f_{max} in the case of electrode polarization. Thus, $f_{MWS}=f_i$ in the first case while $f_{MWS}=f_{max}$ in the second one. This behavior is exemplified in Figure 17, where the characteristic frequencies of these two phenomena are shown in dependence on the volume fraction Φ. For electrode polarization, the parameter Φ is characterized by values in the range of 10^{-5} (because the thickness of the interfacial layers formed in contact with the measurement electrodes is in the nanometer range), while in the case of interfacial polarization measured in bi-layer structures, the two phases have thickness on the same

order of magnitude (thus, Φ shows a value in the decade centered on 0.5). In conclusion, a fundamentally different inter-relation between the characteristic frequencies is found for these two phenomena of electrical polarization, although both of them can be fully described by using the same mathematical formalism represented by eq.15. The analysis of the scaling laws could therefore represent a powerful means to discriminate different phenomena of electrical polarization. This can be extremely useful in understanding the dielectric response of complex materials (heterogeneous materials, multiphase materials, composite materials, etc.), where several dielectric peaks of different origins (molecular fluctuations, interfacial polarization, electrode polarization) can be observed in the global dielectric response.

5.2 Measuring the conductivity of materials without a direct electrical contact

In the standard approach, measuring the conductivity of materials implies a direct contact between the measurement electrodes and the surface of the samples under study. However, in many situations, the ability of measuring the conductivity without employing a direct contact between the electrodes and the samples can turn out to be extremely useful. A contact-less measurement of conductivity would be useful, for instance, when the sample is undergoing a large mechanical deformation. Furthermore, a contact-less conductivity measurement can be useful as well for in-situ investigations when the samples are subjected to external stimuli such as a vapor treatment, etc...The non-conventional way of measuring the conductivity using a contact-less approach can be carried-out with the help of the phenomenon of electrode polarization. The basic principle is illustrated in Figure 18. Measuring the conductivity of a material using an air gap geometry leads to global dielectric response consisting of two different contributions: the contribution of the conductive phase (the materials under study) and the contribution of the insulating phase (the air gap). Due the dielectric contrast between the two phases, a MWS peak appears in the global dielectric loss. For a detailed analysis of its frequency position in dependence on the conductivity value, the dielectric response in an air-gap geometry must be first calculated as:

$$\varepsilon_{net}^{*} = \frac{\varepsilon_{cond}^{*}\varepsilon_{ins}^{*}}{\Phi\varepsilon_{cond}^{*} + (1-\Phi)\varepsilon_{ins}^{*}} \qquad \text{(eq.20)}$$

Where: $\Phi = d_{ins}/L$ represents the volume fraction of insulating phase (the air gap), $\varepsilon_{cond}^{*} = \varepsilon'_{cond} - i\varepsilon''_{cond}$ the complex dielectric function of the conductive phase (the polymer layer) and $\varepsilon_{ins}^{*} = \varepsilon'_{ins} - i\varepsilon''_{ins}$ the complex dielectric function of the insulating phase.

Separating the real and the imaginary part leads to:

$$\varepsilon'_{net} = \frac{\left[\left(\varepsilon'_{ins}\varepsilon'_{cond} - \varepsilon''_{ins}\varepsilon''_{cond}\right)\left((1-\Phi)\varepsilon'_{ins} + \Phi\varepsilon'_{cond}\right) + \left(\varepsilon''_{ins}\varepsilon'_{cond} + \varepsilon'_{ins}\varepsilon''_{cond}\right)\left((1-\Phi)\varepsilon''_{ins} + \Phi\varepsilon''_{cond}\right)\right]}{\left[(1-\Phi)\varepsilon'_{ins} + \Phi\varepsilon'_{cond}\right]^2 + \left[(1-\Phi)\varepsilon''_{ins} + \Phi\varepsilon''_{cond}\right]^2}$$

(eq.21a)

$$\varepsilon''_{net} = \frac{\left[\left(\varepsilon''_{ins}\varepsilon'_{cond} + \varepsilon'_{ind}\varepsilon''_{cond}\right)\left((1-\Phi)\varepsilon'_{ins} + \Phi\varepsilon'_{cond}\right) - \left(\varepsilon'_{ins}\varepsilon'_{cond} - \varepsilon''_{ins}\varepsilon''_{cond}\right)\left((1-\Phi)\varepsilon''_{ins} + \Phi\varepsilon''_{cond}\right)\right]}{\left[(1-\Phi)\varepsilon'_{ins} + \Phi\varepsilon'_{cond}\right]^2 + \left[(1-\Phi)\varepsilon''_{ins} + \Phi\varepsilon''_{cond}\right]^2}$$

(eq.21b)

The MWS interfacial polarization is manifested as a peak appearing in the dielectric loss. Its frequency position can therefore be calculated by solving the equation:

$$\frac{\partial(\log \varepsilon'')}{\partial(\log f)} = 0 \qquad \text{(eq.22)}$$

This leads to:

$$f_{MWS}^{2} = \frac{\sqrt{(3\beta\gamma - \alpha\delta)^2 - 4\alpha\beta\gamma\delta} - (3\beta\gamma - \alpha\delta)}{2\alpha\gamma} \qquad \text{(eq.23)}$$

With:

$$\alpha = \left[\left(\sigma_{ins}\varepsilon'_{cond} + \sigma_{cond}\varepsilon'_{ins}\right)\left[(1-\Phi)\varepsilon'_{ins} + \Phi\varepsilon'_{cond}\right] - \varepsilon'_{ins}\varepsilon'_{cond}\left[(1-\Phi)\sigma_{ins} + \Phi\sigma_{cond}\right]\right]/(2\pi\varepsilon_0) \qquad \text{(eq.23a)}$$

$$\beta = \left[\sigma_{ins}\sigma_{cond}\left[(1-\Phi)\sigma_{ins} + \Phi\sigma_{cond}\right]\right]/(2\pi\varepsilon_0)^3 \quad \text{(eq.23b)}$$

$$\delta = \left[(1-\Phi)\sigma_{ins} + \Phi\sigma_{cond}\right]^2/(2\pi\varepsilon_0)^2 \quad \text{(eq.23c)}$$

$$\gamma = \left[(1-\Phi)\varepsilon'_{ins} + \Phi\varepsilon'_{cond}\right]^2 \quad \text{(eq.23d)}$$

Considering that $\sigma_{ins}=0$, one gets an analytical expression relating the frequency position of the MWS interfacial polarization to the conductivity value of the polymer layer:

$$f_{MWS} = \frac{\Phi\sigma_{DC}}{2\pi\varepsilon_0\left[(1-\Phi)\varepsilon'_{ins} + \Phi\varepsilon'_{cond}\right]} \quad \text{(eq.24)}$$

The validity of this formula has been verified by measuring bi-layer polymer samples consisting in one conductive and an air gap. In a broad temperature range, an excellent agreement is found between the measured values of conductivity and those calculated using the above formula (Figure 18). Our approach is thereby validated for measuring the conductivity in an air-gap geometry, without a direct contact between the electrodes and the surface of the measured sample.

6. Conclusions

In the present work, the scaling laws governing the electrical and dielectric behavior of composite materials consisting of two different dielectric phases have been studied. For this purpose, the characteristic frequencies describing the global dielectric behavior have been analyzed in dependence on morphology, conductivity, volume fraction, orientation of fillers, form factor and presence of interphases exhibiting different gradients of local properties. A first theoretical approach was demonstrated to evidence the impact of local gradients of properties existing in the interphases formed between two distinct dielectric regions present in a composite material. Two applications of our analysis of scaling laws were demonstrated: (i) discriminating different phenomena of electrical polarization (interfacial polarization vs. electrode polarization); (ii) measuring conductivity of materials without employing a direct electrical contact between the electrodes and the samples under

investigation. Our study delivered thus a useful and necessary analysis of the dielectric behavior of composite materials, where interfacial polarization effects play a major role.

Acknowledgements

The authors would like to thank Dr. Gisèle Boiteux for her precious advices and kind assistance during this study.

Data availability

The data that support the findings of this study are available from the corresponding author upon reasonable request.

References:

1. Kremer F and Schönhals A. Broadband Dielectric Spectroscopy, Berlin: Springer, 2003.

2. Nasedkin A, Cerveny S, and Swenson J. Molecular Insights into Dipole Relaxation Processes in Water–Lysine Mixtures. J. Phys. Chem. B 2019; 123: 6056–6064
3. Sawickia B, Tomaszewicz E, Groń T ,Berkowski M ,.Głowacki M, Oboa M, Kusz J and Pawlus S. Dipole relaxation process and giant dielectric permittivity in Eu3+-doped CdMoO4 single crystal. Journal of Materiomics 2021; 7: 845–857
4. Ouled Ltaief A, Ghorbel N, Benhamou K, Arous M, Kaddami H and Kallel A. Impact of cellulose nanocrystals reinforcement on molecular dynamics and dielectric properties of PCL-based polyurethane. Polymer Composites. 2021; 42: 2737– 2750
5. Svirskas S, Balčiūnas S, Šimėnas M, Usevičius G, Kinka M, Velička M, Kubicki D, Escobar Castillo M, Karabanov A, V. Shvartsman V, de Rosário Soares M, Šablinskas V, N. Salak A, C. Lupascu D and Banys J. Phase transitions, screening and dielectric response of CsPbBr3. The Journal of Materials Chemistry A. 2020, 8: 14015– 14022
6. Serghei A, Tress M and Kremer F. The glass transition of thin polymer films in relation to the interfacial dynamics. J. Chem. Phys. 2009; 131: 154904
7. Tress M, Erber M, Mapesa E U, Huth H, Muller J, Serghei A, Schick C, Eichhorn K-J, Voit B and Kremer F. Glassy Dynamics and Glass Transition in Nanometric Thin Layers of Polystyrene. Macromolecules 2010; 43: 9937–44.
8. Krause C, Sangoro J R, Iacob C and Kremer, F. Charge Transport and Dipolar Relaxations in Imidazolium-Based Ionic Liquids. J. Phys. Chem. B 2010; 114: 382–86
9. Tarlton T, Brown J, Beach B and Derosa P A. A stochastic approach towards a predictive model on charge transport properties in carbon nanotube composites. Comp Part B: Eng 2016; 100: 56–67.
10. Hussan K. P. S, Thayyil M S, Rajan V K and Antony A. The Interplay between Charge Transport and CO2 Capturing Mechanism in [EMIM][SCN] Ionic Liquid: A Broadband Dielectric Study. J. Phys. Chem. B 2019; 123: 6618–6626
11. Belgaroui E and Kallel A. Bipolar electronic charge transport model under trap density Gaussian spatial distribution: Application to dielectric polymer interfaces. Physica Scripta 2019; 94: 105819.

12. Serghei A, Sangoro J R and Kremer F. Broadband dielectric spectroscopy on electrode polarisation and its scaling; in Electrical Phenomena at Interfaces and Biointerfaces: Fundamentals and Applications in Nano-, Bio-, and Environmental Science, Ohshima H, 2012, pp 241–273.
13. Serghei A, Tress M, Sangoro J R and Kremer F. Electrode polarization and charge transport at solid interfaces. Phys. Rev. B 2009; 80: 184301
14. Samet M, Kallel A, Kallel-Elloumi A, Drockenmuller E and Serghei A. Exchange process in the dielectric loss of molecular and macromolecular ionic conductors in the interfacial layers formed by electrode polarization effects. J. Phys. Chem. B 2019; 123: 8532–8542
15. Lin X, Fan L, Ren D, Jiao Z, Coates P and Yan W. Enhanced dielectric properties of immiscible poly (vinylidene fluoride)/low density polyethylene blends by inducing multilayered and orientated structures. Comp Part B: Eng 2017, 114: 58–68
16. Kreit L, Bouknaitir I, Zyane A, et al. Electrical conductivity and dielectric relaxation studies of biocomposites based on green microcrystalline cellulose-reinforced vinyl resin matrix. J Compos Mater 2019; 53: 2801–2808
17. Samet M, Kallel A and Serghei A. Polymer bilayers with enhanced dielectric permittivity and low dielectric losses by Maxwell–Wagner–Sillars interfacial polarization: Characteristic frequencies and scaling laws. J. Appl. Polym. Sci. 2019; 136: 47551
18. Ren D, Li K, Chen L, Chen S, Han M, Xu M and Liu X. Modification on glass fiber surface and their improved properties of fiber-reinforced composites via enhanced interfacial properties. Comp Part B: Eng 2019; 177: 107419
19. Gorrasia G, Bugattia V, Milone C, Mastronardo E, Piperopoulos E, Iemmo, L Di and Bartolomeo A. Effect of temperature and morphology on the electrical properties of PET/conductive nanofillers composites. Comp Part B: Eng 2018; 135: 149–54
20. Carroll B, Cheng S and Sokolov A P. Analyzing the Interfacial Layer Properties in Polymer Nanocomposites by Broadband Dielectric Spectroscopy. Macromolecules 2017; 50: 6149–6163

21. Ben Amor I, Arous M and Kallel A. Interfacial polarization phenomena in palm tree fiber-reinforced epoxy and polyester composites. Journal of composite materials 2013; 48: 2631–2638
22. Belhimria R, Samir Z, Boukheir S, Soreto Teixeira, S, Achour, Anson-Casaos, M E A, Gonzalez-Dominguez J M, Costa L C and El Hasnaoui M. Thermal and dielectric properties of carbon nanotubes/graphite/polyester ternary composites. Journal of composite materials 2021; 55: 3741–3750
23. Butt H J, Duran H, Egger W, Faupel F, Harmandaris V, Harms S, Johnston K, Kremer K, Lin F Y, Lue L, Ohrt C, Raetzke K, Ravelli L, Steffen W and Vianna S D B. Interphase of a polymer at a solid interface. Macromolecules 2014; 47: 8459–8465
24. Brown W F. Mixture Permittivities. J. Chem. Phys.1955; 23: 1514-1517
25. Van Beek L K H. Dielectric Behavior of Heterogeneous Systems, In Progress in Dielectric, edited by J.B. Birks, Heywood Books, London. 1967. pp. 69-114
26. Sheu S –Y, Kumar S and Cukier R I. Simulation of the dielectric constant of a composite material. Phys. Rev. B 1990; 42: 1431–1438
27. Cukier R I, Sheu S Y and Tobochnik J. Random-walk simulation of the dielectric constant of a composite material. Phys. Rev. B 1990; 42: 5342–5344
28. Priou, A. Dielectric properties of heterogeneous materials, in Progress in electromagnetic research, Amsterdam: North-Holland. 1992. pp. 621–315
29. Tuncer E, Serdyuk Y V and Gubanski S M. Dielectric mixtures: electrical properties and modeling. IEEE Transactions on Dielectrics and Electrical Insulation 2002; 9: 809–828
30. Serdyuk Y V, Podoltsev A D and Gubanski S M. Numerical simulations of dielectric properties of composite material with periodic structure. Journal of Electrostatics 2005; 63: 1073–1091
31. Wang M and Pan N. Numerical analyses of effective dielectric constant of multiphase microporous media. Journal of Applied Physics 2007; 101: 114102
32. Cheng Y, Chen X, Wu K, Wu S, Chen Y and Meng Y. Modeling and simulation for effective permittivity of two-phase disordered composites. Journal of Applied Physics 2008; 103: 034111

33. Ahmadi A and Mosallaei H. Physical configuration and performance modeling of all-dielectric metamaterials. Phys. Rev. B 2008; 77: 045104
34. Cheng L, Zhou J, Xiaozhong H and Li Y. Dielectric properties of continuous fiber reinforced polymer composites: Modeling, validation, and application. Polymer Composites 2017; 39: 4646-4655
35. Doyle T E, Robinson D A, Jones S B, Warnick K H and Carruth B L. Modeling the permittivity of two-phase media containing monodisperse spheres: Effects of microstructure and multiple scattering. Phys. Rev. B 2007; 76: 054203
36. Wang M and Pan N. Predictions of effective physical properties of complex multiphase materials. Materials Science and Engineering 2008; 63: 1–30
37. Galatry L and Gharbi T. Theory of the interfacial polarization between isotropic and neutral dielectric bodies. J. Chem. Phys 1981; 75: 3608–3616
38. Drozdov AD and Christiansen deClaville J. Modeling dielectric permittivity of polymer composites filled with transition metal dichalcogenide nanoparticles. Journal of Composite Materials. 2020; 54: 3841–3855
39. Chen A, Yu Z, Guo R and Bhalla A.S. Calculation of dielectric constant and loss of two-phase composites. Journal of Applied Physics 2003; 93: 347
40. Pal R. On the Electrical Conductivity of Particulate Composites. Journal of composite Material 2007; 41: 2499–2511
41. Maxwell-Garnett J. C. XII. Colours in metal glasses and in metallic films. Philos. Trans. R. Soc. London 1904; 203: 371–385
42. Samet M, Boiteux G, Seytre G, Kallel A and Serghei A. Interfacial polarization in composite materials with spherical fillers: Characteristic frequencies and scaling laws. Colloid Polym. Sci. 2014; 292: 1977–1988
43. Markel V A. Introduction to the Maxwell Garnett approximation: tutorial. Journal of the Optical Society of America A 2016; 33: 1244–1256
44. Asami K. Characterization of heterogeneous systems by dielectric spectroscopy. Prog.Polym. Sci. 2002; 27: 1617–1659

45. Asami K, Hanai T and Koizumi N. Dielectric approach to suspensions of ellipsoidal particles covered with a shell in particular reference to biological Cells. J. Appl. Phys 1980; 19: 359–365
46. Altshuller A P. The shapes of particles from dielectric constant studies of suspensions. J. Phys. Chem 1954; 58: 544-547
47. Fricke H. The Maxwell-Wagner dispersion in a suspension of ellipsoids. J. Phys. Chem.1953; 57: 934-937
48. Macdonald J R and Barbero G. Reanalysis of the electrode polarization in electrolytic cells limited by blocking electrodes Phys. Rev. E 2016; 94: 042608
49. Sanabria H and Miller H J. Relaxation processes due to the electrode-electrolyte interface in ionic solutions. Phys. Rev. E 2006; 74: 051505
50. Samet M, Levchenko V, Boiteux G, Seytre G, Kallel A and Serghei A. Electrode polarization vs. Maxwell-Wagner-Sillars interfacial polarization in dielectric spectra of materials: Characteristic frequencies and scaling laws. J. Chem.Phy. 2015; 42: 194703

Figure captions:

Figure 1: The dielectric loss ε'' of a PVAc layer with a thickness of 100μm **(a,d)** and of a P2VP layer **(b, e)** with a thickness of 100μm, measured separately and together in a bi-layer structure **(c, f),** as function of temperature at a constant frequency of 100Hz **(left graphs)** and as function of frequency at a constant temperature of 120 ^{o}C **(right graphs)**.

Figure 2: The effective permittivity, the effective dielectric loss and the voltage distribution of a bi-layer system consisting of two different dielectric phases (phase A and phase B) having an identical permittivity value ($\varepsilon_A = \varepsilon_B = 3$), an identical thickness $\left(d_A = d_B = 0.1mm\right)$ and showing a difference of 3 orders of magnitude between their dielectric losses (conductivity of phase A $\sigma_A=10^{-8}$ S/cm, conductivity of phase B $\sigma_B=10^{-11}$ S/cm).

Figure 3: The measured impedance values for the experimental data shown in Fig. 1 d, e, f.

Figure 4: The complex dielectric function ($\varepsilon^*_{net}=\varepsilon'_{net} - i\varepsilon''_{net}$) and the complex conductivity function ($\sigma^*_{net}=\sigma'_{net} + i\sigma''_{net}$) of several multiphase materials consisting of an insulating matrix ($\varepsilon'_m= 3$, $\sigma'_m=10^{-12}$ S/cm) and a conductive fillers ($\varepsilon'_f= 3$, $\sigma'_f=10^{-6}$ S/cm) with a fixed volume fraction Φ=20%. Different morphologies were investigated: layered, cylindrical, spherical and ellipsoidal particles, as indicated.

Figure 5: The characteristic frequencies of polarization effects: f_{on}, f_{max}, f_{MWS} and f_i defined in spectra of ε', ε'', the first and the second derivative of ε'.

Figure 6: The complex dielectric function ($\varepsilon^*_{net}=\varepsilon'_{net} - i\varepsilon''_{net}$) and the complex conductivity function ($\sigma^*_{net}=\sigma'_{net} + i\sigma''_{net}$) in dependence on the frequency for different values of the DC-conductivity for multiphase materials consisting of an insulating matrix ($\sigma'_m=10^{-12}$ S/cm) and conductive fillers. The volume fraction is Φ =20%. For three different morphologies: Layered, spherical and ellipsoidal.

Figure 7: (a) The characteristic frequencies f_{max}, f_{on}, f_i and f_{MWS} (determined from the data presented in Fig. 6) **(b)** The ratio $f_i^2/(f_{max} \times f_{on})$ **(c)** The plateau values of ε'_{net}at low frequencies, are plotted as a function of the DC-conductivity of the fillers ($\sigma_{cond}=\sigma_{DC}$); for three different morphologies of multiphase materials (layered, spherical and ellipsoidal), as indicated.

Figure 8: The complex dielectric function ($\varepsilon^*_{net}=\varepsilon'_{net} - i\varepsilon''_{net}$) and the complex conductivity function ($\sigma^*_{net}=\sigma'_{net} + i\sigma''_{net}$) in dependence on the frequency at different values of volume fraction Φ. Three different morphologies of multiphase materials were investigated (layered, spherical and ellipsoidal). Conductivity values of 10^{-12} S/cm and 10^{-6} S/cm were assumed for the insulating matrix and the conductive fillers, respectively.

Figure 9: (upper graphs) The characteristic frequencies f_{on}, f_{max}, f_i, and f_{MWS}(determined from the data presented in Fig. 8) **(middle graphs)** The ratio $f_i^2/(f_{on}xf_{max})$ **(lower graphs)** The plateau values of ε'_{net} at low frequencies, as a function of the volume fraction of the fillers; for three different morphologies of multiphase materials (layered, spherical and ellipsoidal), as indicated.

Figure 10: The complex permittivity ($\varepsilon^*_{net} =\varepsilon'_{net} -i\varepsilon''_{net}$) and the complex conductivity ($\sigma^*_{net}=\sigma'_{net} +i\sigma''_{net}$) of composite material consisting of a host insulating matrix ($\sigma'_m=10^{-12}$ S/cm) filled with conductive ellipsoidal particles ($\sigma'_f= 10^{-6}$ S/cm and Φ=10%) were simulated. Three different orientations of the ellipsoidal fillers were considered: (i) Random orientation, (ii) oriented parallel to E direction (iii) perpendicular to E direction.

Figure 11: The complex permittivity ($\varepsilon^*_{net} =\varepsilon'_{net} -i\varepsilon''_{net}$) and the complex conductivity ($\sigma^*_{net}=\sigma'_{net} +i\sigma''_{net}$) of composite material consisting of a host insulating matrix (with a conductivity value of 10^{-12} S/cm) filled with conductive ellipsoidal particles **(left graphs)** with a fixed volume fraction Φ=10% and at different DC-conductivity values of the fillers; **(right graphs)** as a function of the volume fraction of fillers with a constant conductivity

value of 10^{-6} S/cm. Three different orientations of the ellipsoidal fillers were estimated (Random orientation, oriented parallel and perpendicular to E direction).

Figure 12: (upper graphs) Characteristic frequencies f_{on}, f_{max}, f_i and f_{MWS} (determined from the data presented in Fig. 11 left) **(middle graphs)** The ratio $f_i^2/(f_{on}xf_{max})$ plotted as a function of the DC-conductivity of the fillers at fixed volume fraction Φ =10%. **(lower graphs)** The characteristic frequencies f_{on}, f_{max}, f_i and f_{MWS} (determined from the data presented in Fig. 11 right) as a function of the volume fraction of the fillers. All three different orientations were investigated, as indicated.

Figure 13: The plateau values of ε'_{net} in low frequency range (form the data presented in fig.12 right) in dependence on the volume fraction of the fillers for three different orientations of the ellipsoidal particles.

Figure 14: Complex dielectric function of composite materials with ellipsoidal fillers of different values of form factor q. The Conductivity values of 10^{-12} S/cm and 10^{-6} S/cm were considered for the insulating matrix and the conductive fillers, respectively. The volume fraction is Φ =20%.

Figure 15: The characteristic frequencies as a function of the form factor q, in log-log plot.

Figure 16: (upper graphs) Schematic presentation of **(a)** two phases model **(b)** three phases model with interphase showing a gradient of properties.
(lower graph) Complex permittivity and complex conductivity of bi-phases material showing different situations of gradient of properties at interphases: (i) without any gradients of properties; (ii) interphase with a constant local properties (iii) interphase with a linear gradients in the local properties; (iv) interphase with an exponential gradients in the local properties.

Figure 17: (upper graphs) The global dielectric properties of a system consisting of two phases of different conductivity, calculated using formula (eq. 20) for two different values of the volume fraction x: **(left graph)** $x=10^{-5}$, $\sigma_{ins}=10^{-12}$ S/cm, $\sigma_{cond}=10^{-4}$ S/cm, $\varepsilon_{ins}=3$, $\varepsilon_{cond}=3$; **(right graph)** x=0.5, $\sigma_{ins}=10^{-12}$ S/cm, $\sigma_{cond}=10^{-8}$ S/cm, $\varepsilon_{ins}=3$, $\varepsilon_{cond}=3$ **(lower graphs)** The characteristic frequencies f_{on}, f_{max}, f_{MWS} and f_i as a function of $x=d_{ins}/L$.

Figure 18: (a) The dielectric loss of a polymer layer (PVAc blend with 20%v EMPy[TF2N], thickness of 200μm)measured in the conventional geometry(between two electrodes) and using an air-gap geometry (the upper electrode do not touch the surface of the sample under investigation). **(b)** The conductivity values σ_{DC} of the polymer film (PVAc blend with 20%v EMPyr[TF2N]) vs. inverse temperature, as measured and as calculated using the formula (eq.24).

Figures:

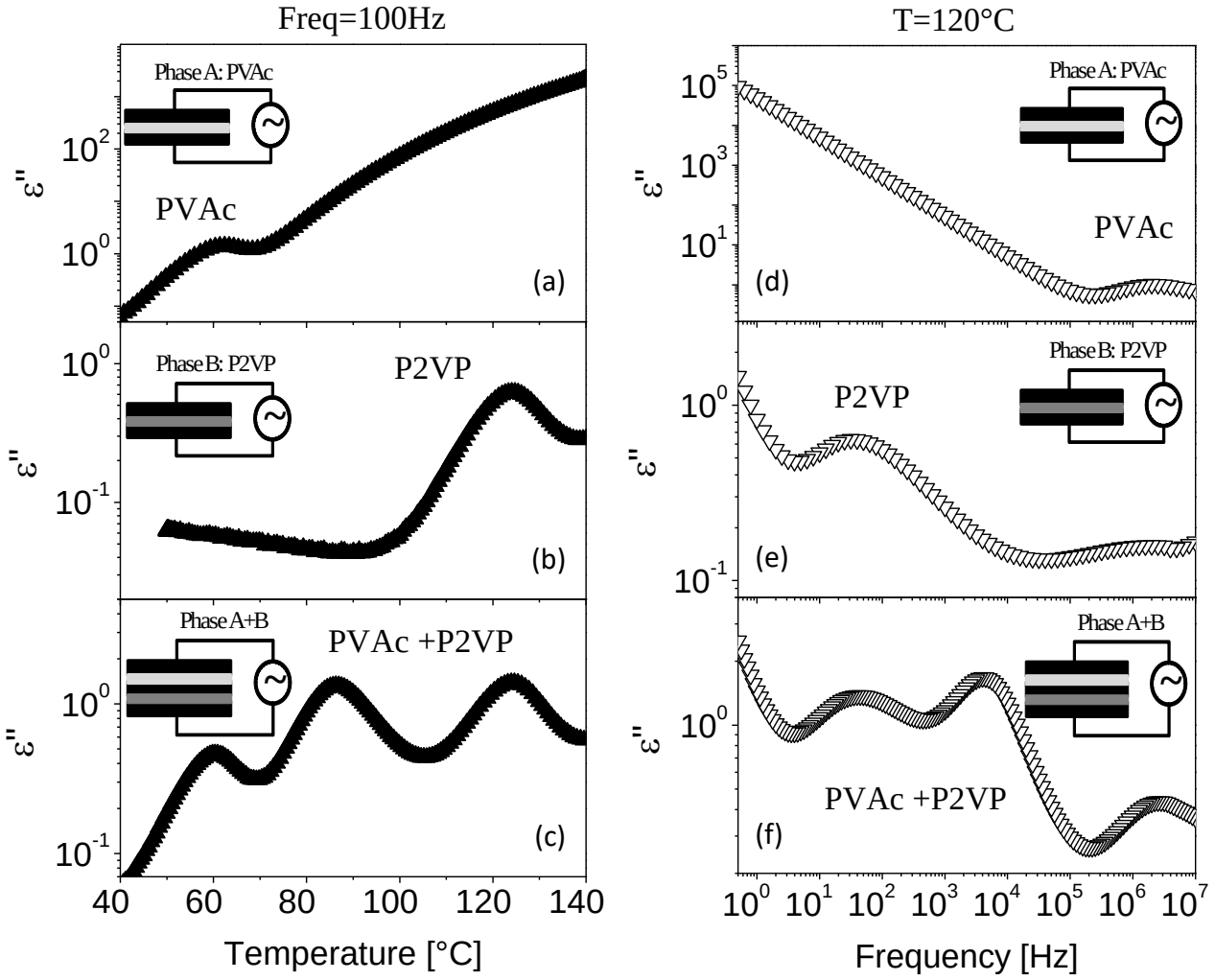
Freq=100Hz
T=120°C
Phase A: PVAc
PVAc
(a)
Phase B: P2VP
P2VP
(b)
Phase A+B
PVAc +P2VP
(c)
(d)
(e)
(f)
ε"
Temperature [°C]
Frequency [Hz]

Figure 1

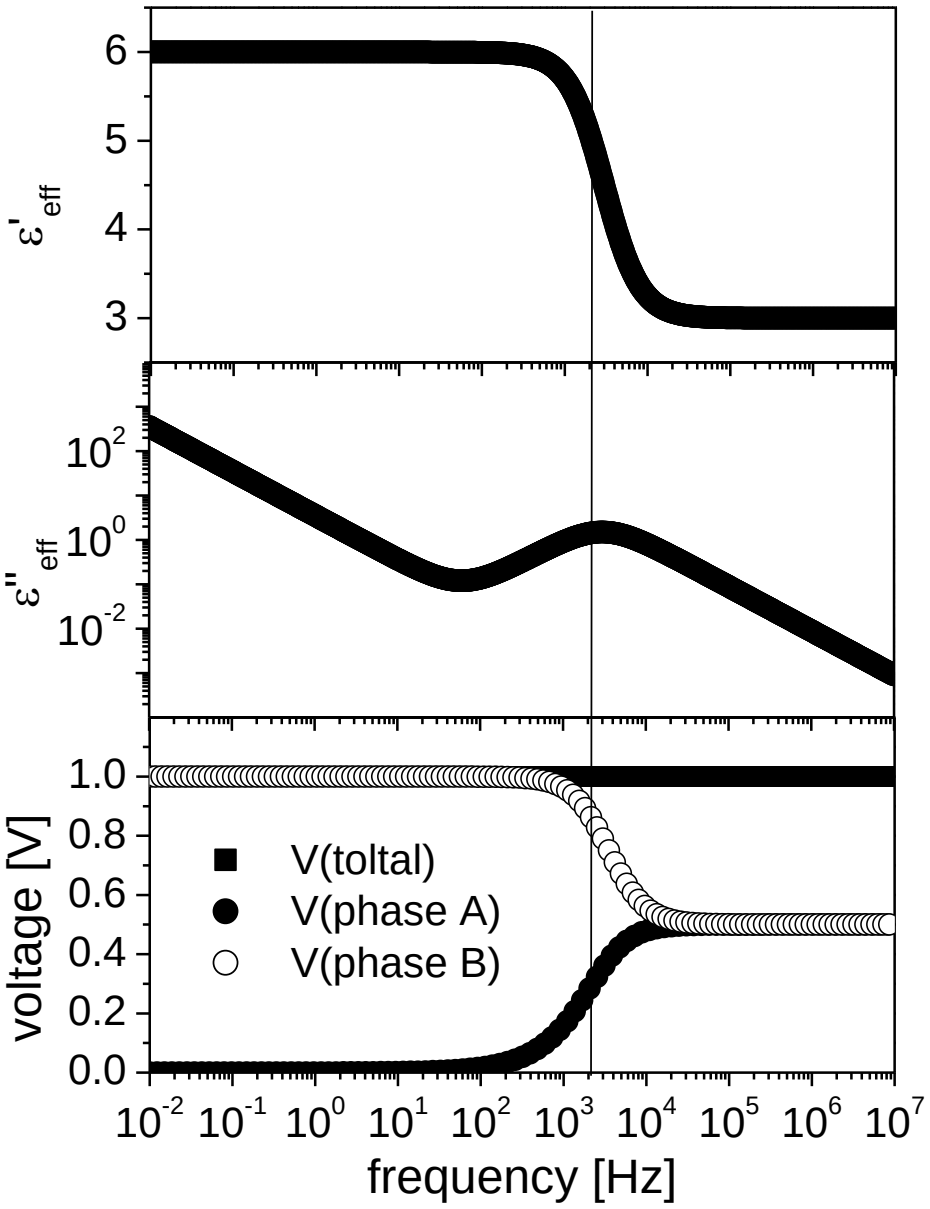
6
5
4
3
ε'eff
10^2
10^0
10^-2
ε''eff
1.0
0.8
0.6
0.4
0.2
0.0
voltage [V]
V(toltal)
V(phase A)
V(phase B)
10^-2 10^-1 10^0 10^1 10^2 10^3 10^4 10^5 10^6 10^7
frequency [Hz]

Figure 2

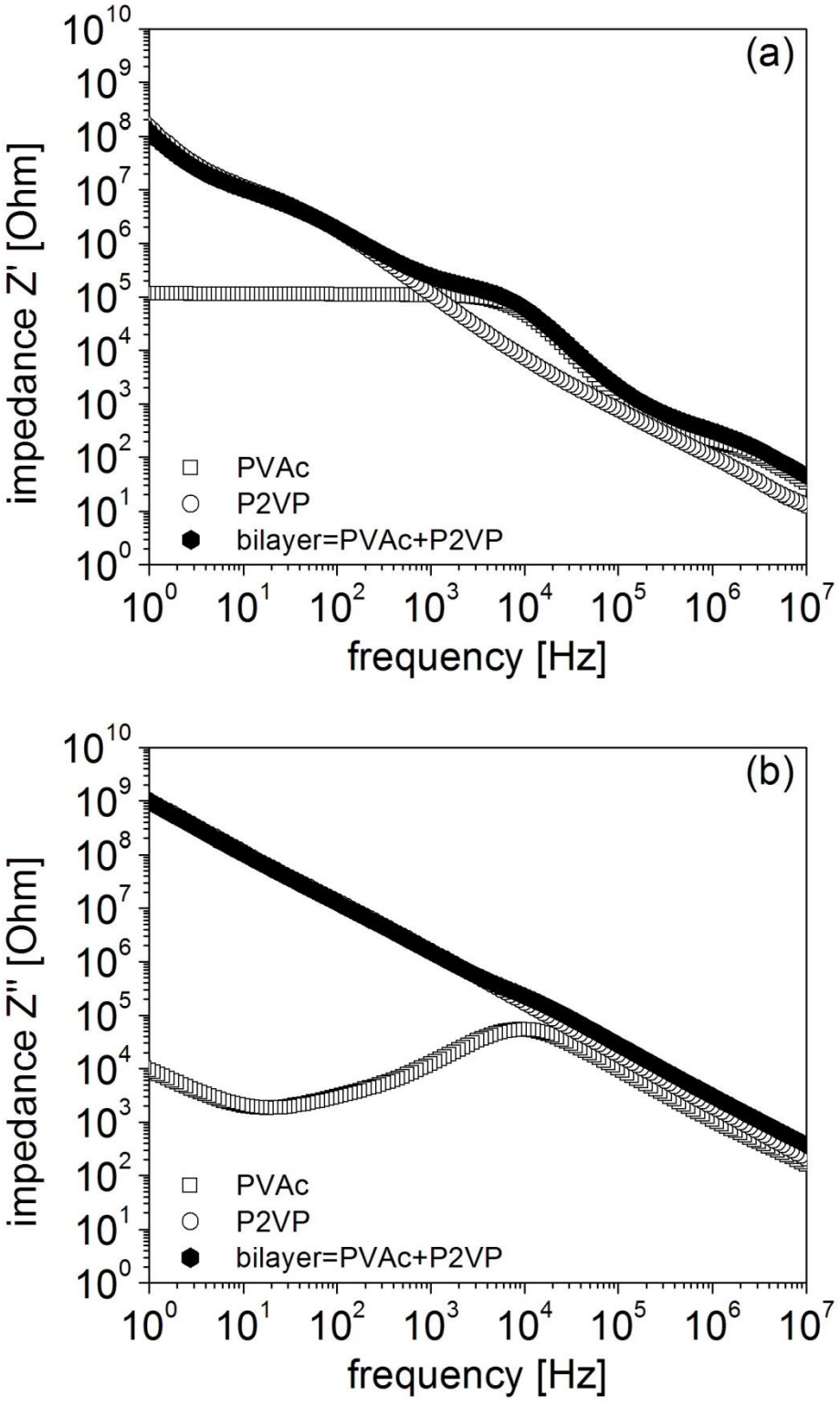
(a)
impedance Z' [Ohm]
frequency [Hz]
PVAc
P2VP
bilayer=PVAc+P2VP
(b)
impedance Z'' [Ohm]
frequency [Hz]
PVAc
P2VP
bilayer=PVAc+P2VP

Figure 3

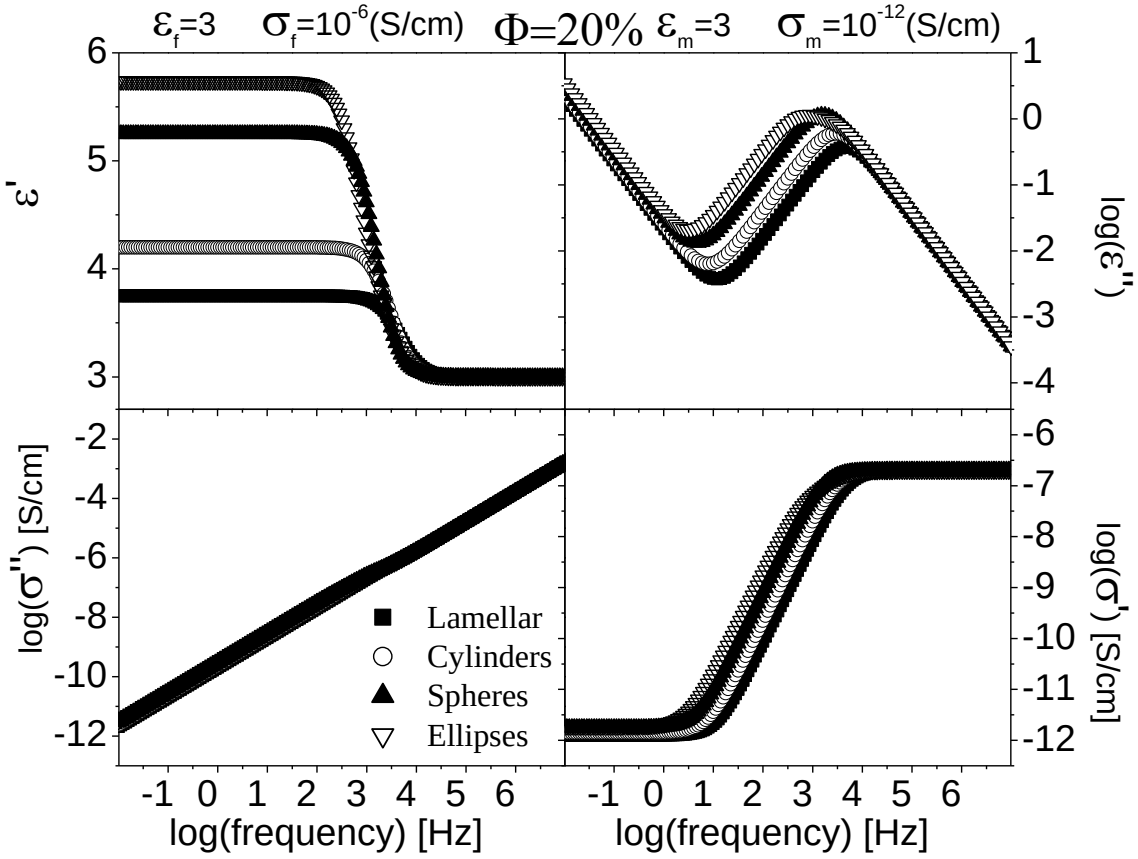
εf=3 σf=10-6(S/cm) Φ=20% εm=3 σm=10-12(S/cm)
ε'
log(ε'')
log(σ'') [S/cm]
log(σ') [S/cm]
log(frequency) [Hz]
log(frequency) [Hz]
Lamellar
Cylinders
Spheres
Ellipses

Figure 4

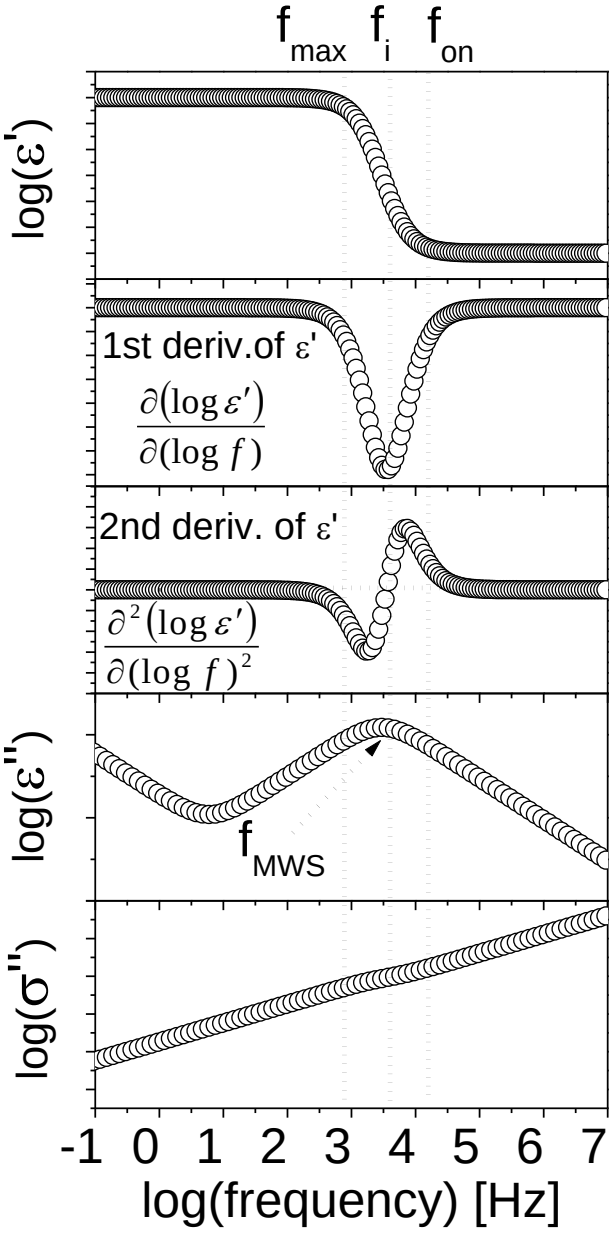
f_max f_i f_on
log(ε')
1st deriv.of ε'
∂(log ε')/∂(log f)
2nd deriv. of ε'
∂²(log ε')/∂(log f)²
log(ε'')
f_MWS
log(σ'')
-1 0 1 2 3 4 5 6 7
log(frequency) [Hz]

Figure 5

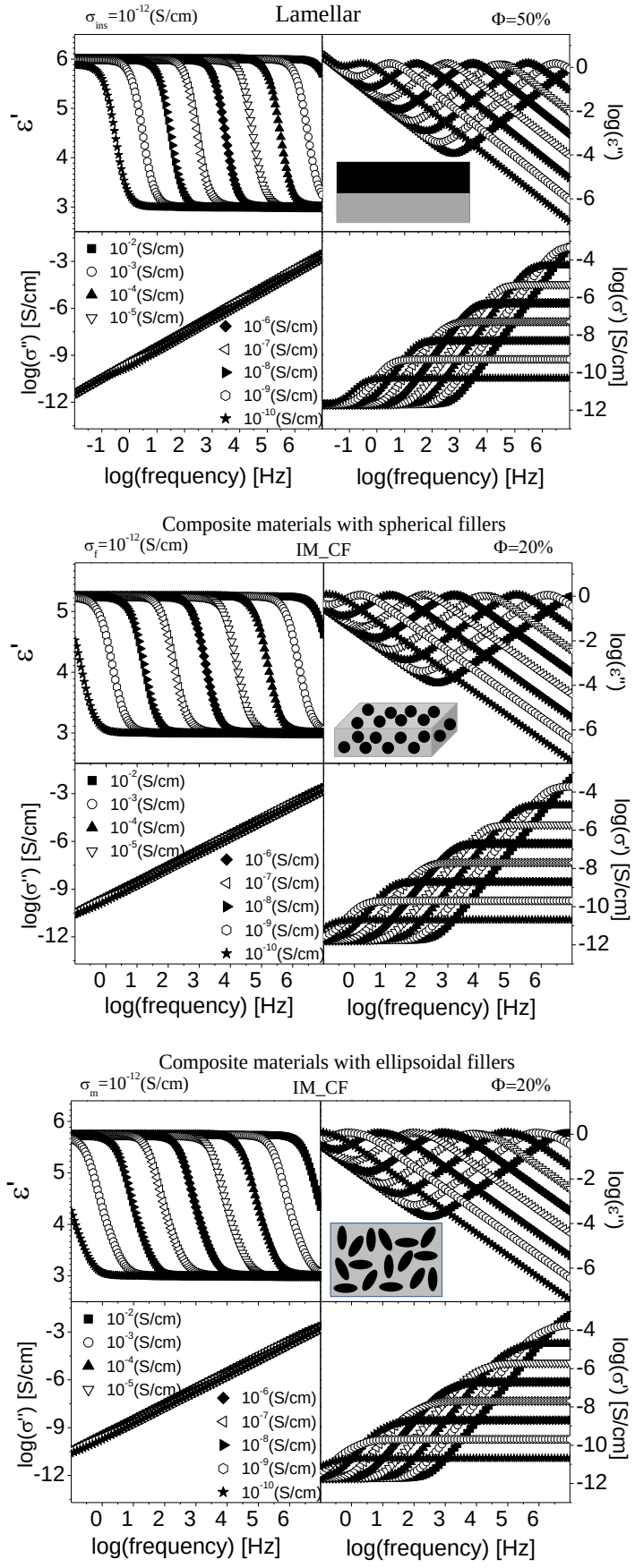
σins=10-12(S/cm)
Lamellar
Φ=50%
ε'
log(ε")
log(σ") [S/cm]
log(σ') [S/cm]
10-2(S/cm)
10-3(S/cm)
10-4(S/cm)
10-5(S/cm)
10-6(S/cm)
10-7(S/cm)
10-8(S/cm)
10-9(S/cm)
10-10(S/cm)
log(frequency) [Hz]
log(frequency) [Hz]
Composite materials with spherical fillers
σf=10-12(S/cm)
IM_CF
Φ=20%
ε'
log(ε")
log(σ") [S/cm]
log(σ') [S/cm]
10-2(S/cm)
10-3(S/cm)
10-4(S/cm)
10-5(S/cm)
10-6(S/cm)
10-7(S/cm)
10-8(S/cm)
10-9(S/cm)
10-10(S/cm)
log(frequency) [Hz]
log(frequency) [Hz]
Composite materials with ellipsoidal fillers
σm=10-12(S/cm)
IM_CF
Φ=20%
ε'
log(ε")
log(σ") [S/cm]
log(σ') [S/cm]
10-2(S/cm)
10-3(S/cm)
10-4(S/cm)
10-5(S/cm)
10-6(S/cm)
10-7(S/cm)
10-8(S/cm)
10-9(S/cm)
10-10(S/cm)
log(frequency) [Hz]
log(frequency) [Hz]

Figure 6

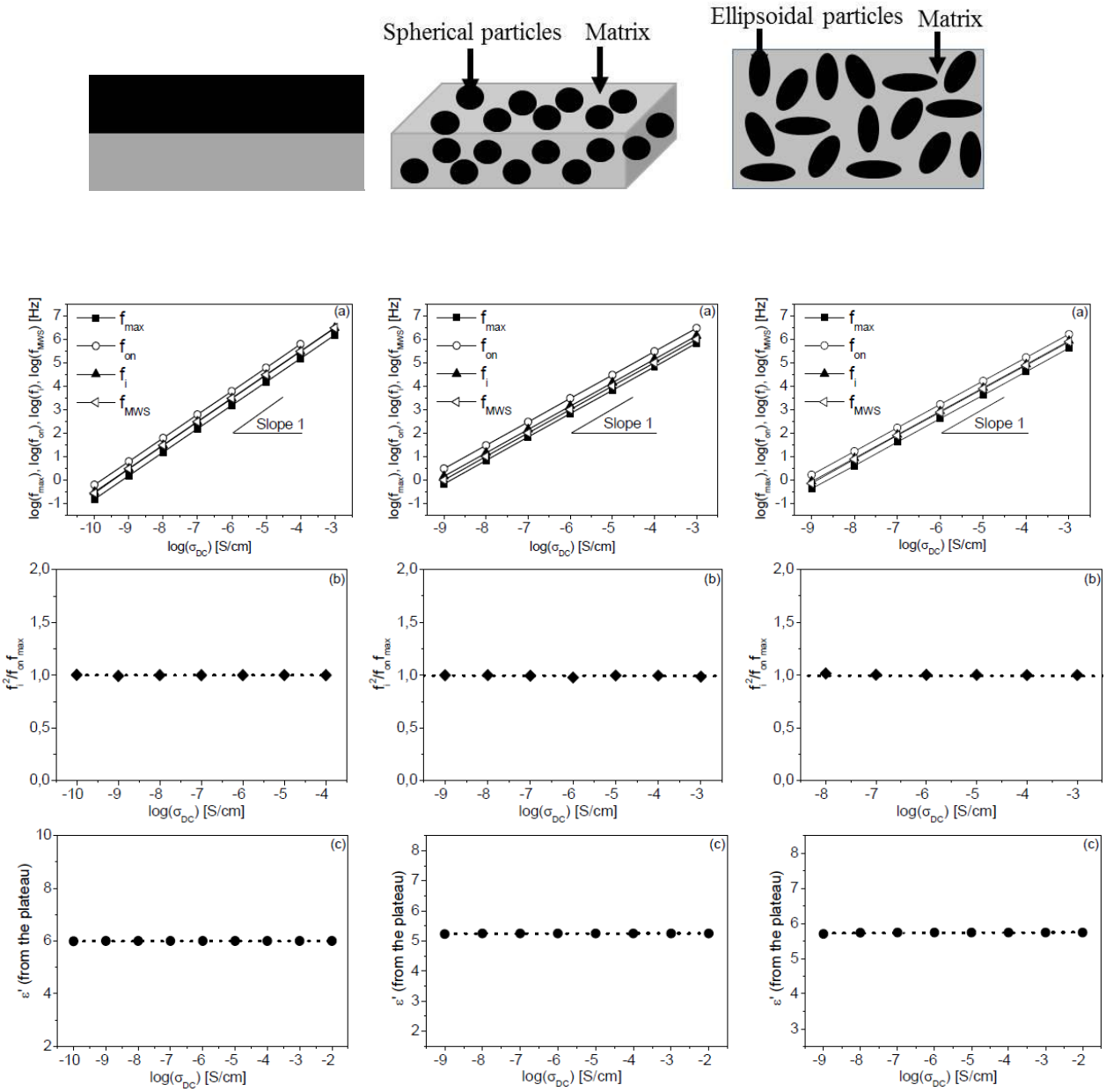
Spherical particles
Matrix
Ellipsoidal particles
Matrix
(a)
(b)
(c)
Slope 1
log(σDC) [S/cm]
ε' (from the plateau)

Figure 7

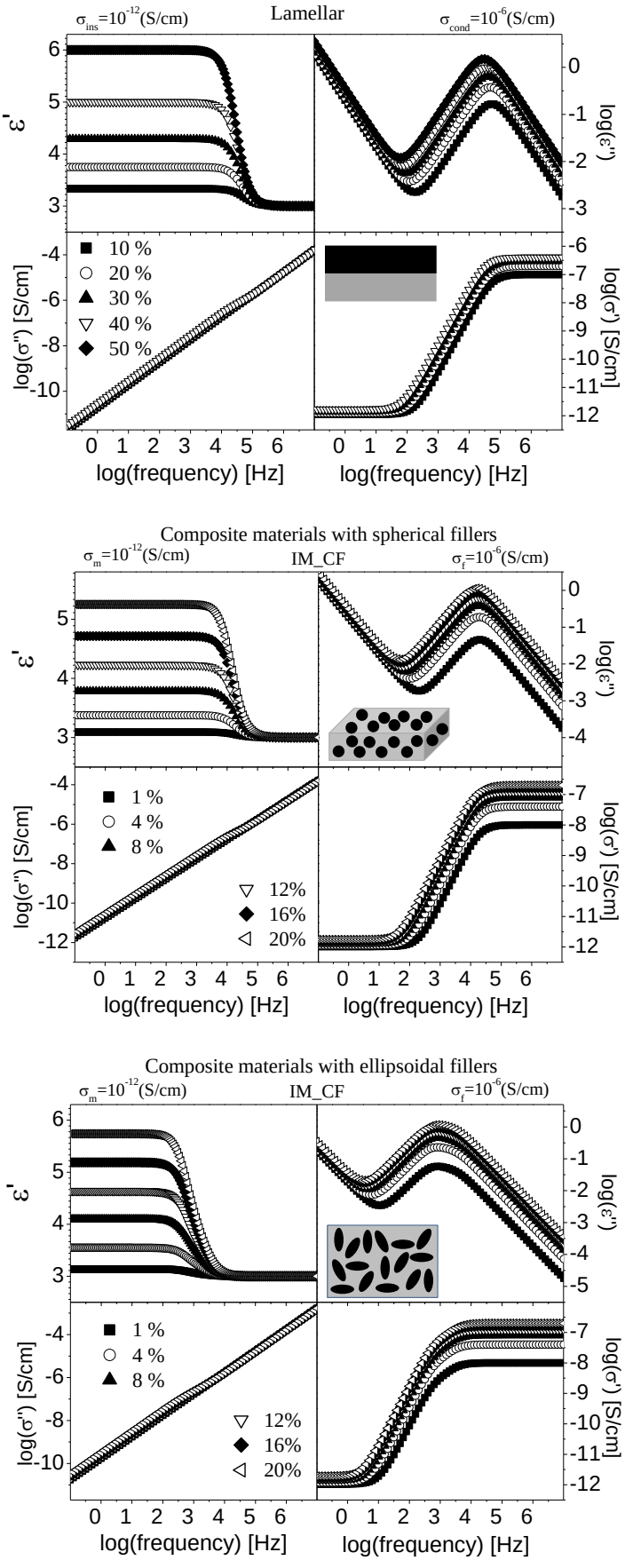
Lamellar
σins=10-12(S/cm)
σcond=10-6(S/cm)
ε'
log(ε")
log(σ") [S/cm]
log(σ') [S/cm]
10 %
20 %
30 %
40 %
50 %
log(frequency) [Hz]
log(frequency) [Hz]
Composite materials with spherical fillers
σm=10-12(S/cm)
IM_CF
σf=10-6(S/cm)
1 %
4 %
8 %
12%
16%
20%
Composite materials with ellipsoidal fillers

Figure 8

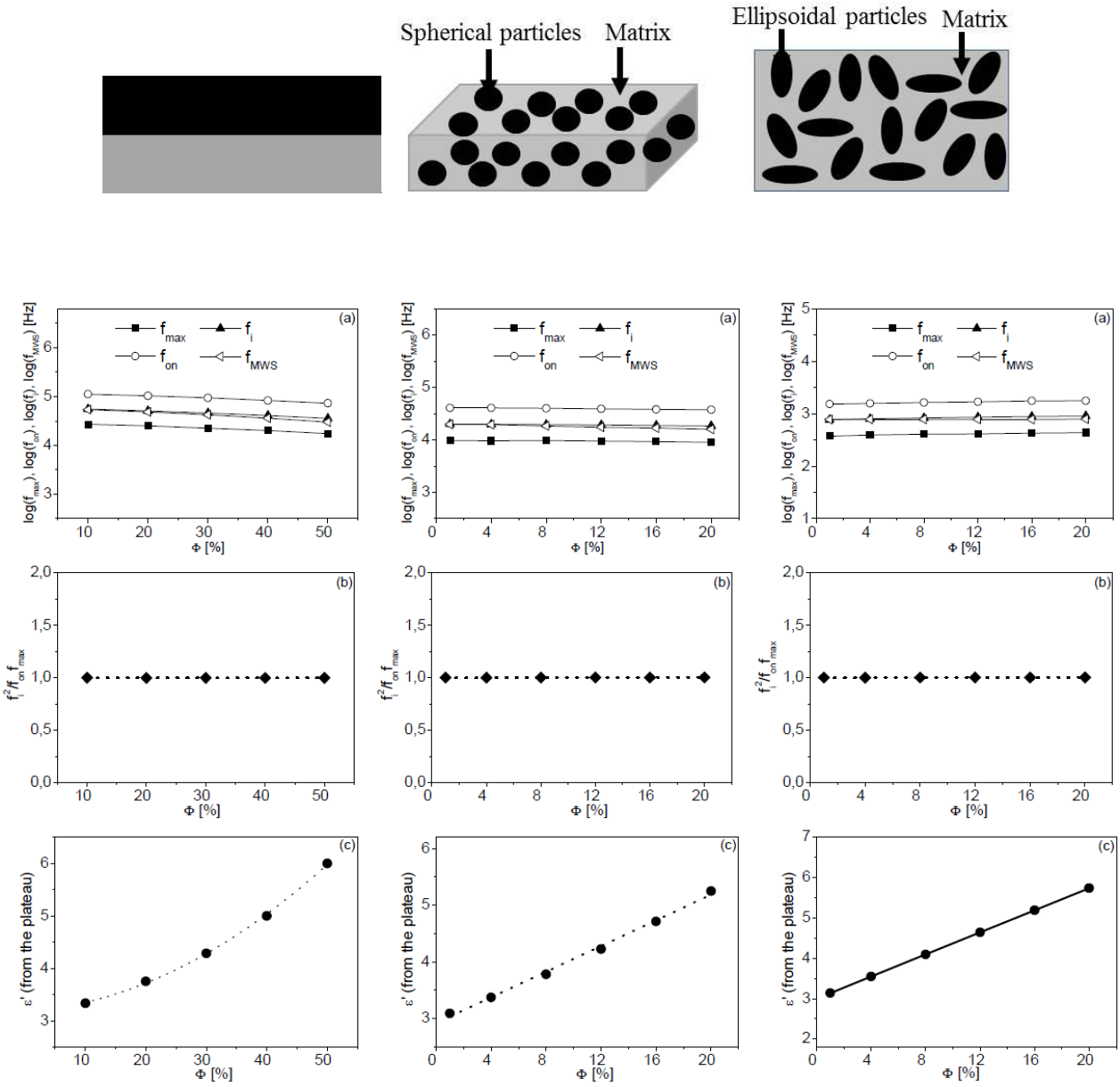
Spherical particles
Matrix
Ellipsoidal particles
Matrix
(a)
(b)
(c)
Φ [%]
ε' (from the plateau)

Figure 9

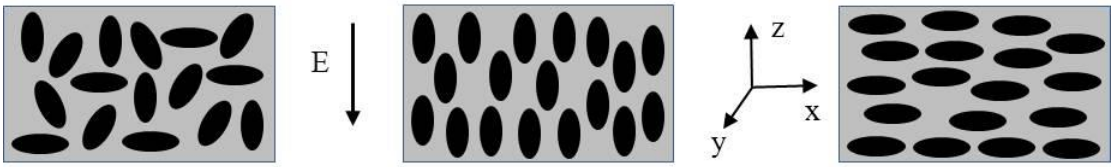
E
z
x
y

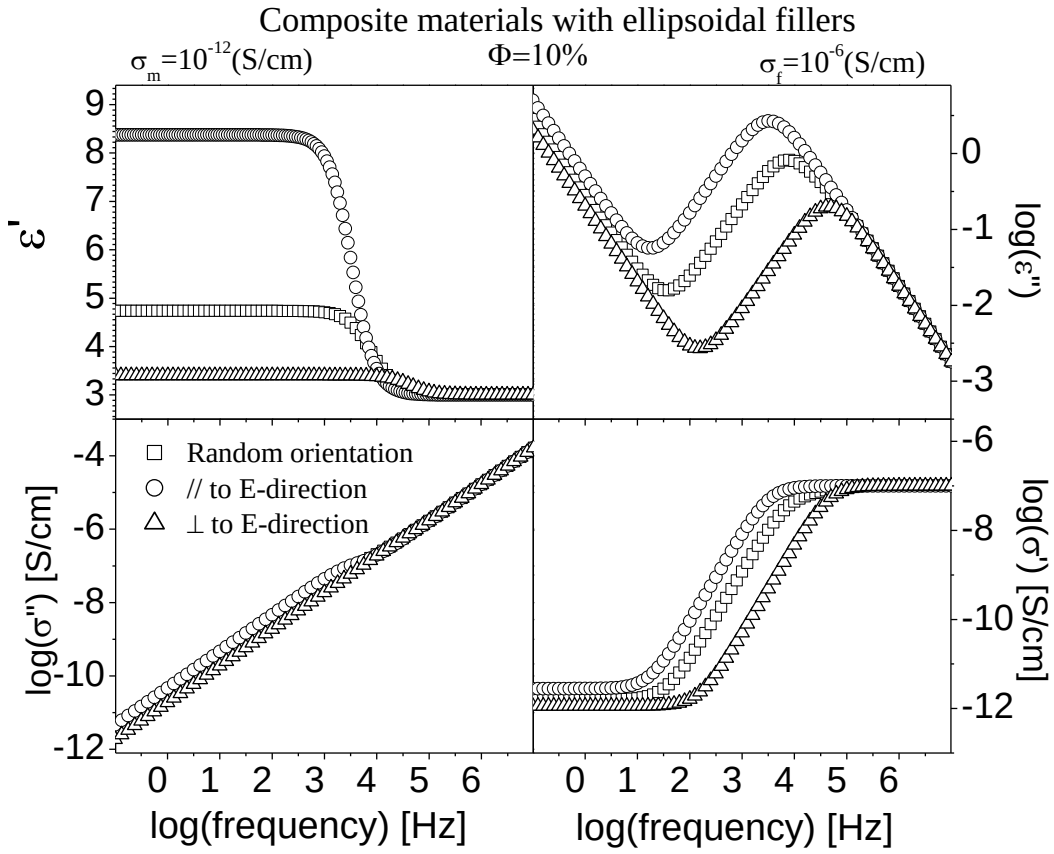
Composite materials with ellipsoidal fillers
σm=10-12(S/cm)
Φ=10%
σf=10-6(S/cm)
ε'
log(ε")
log(σ") [S/cm]
log(σ') [S/cm]
Random orientation
// to E-direction
⊥ to E-direction
log(frequency) [Hz]
log(frequency) [Hz]

Figure 10

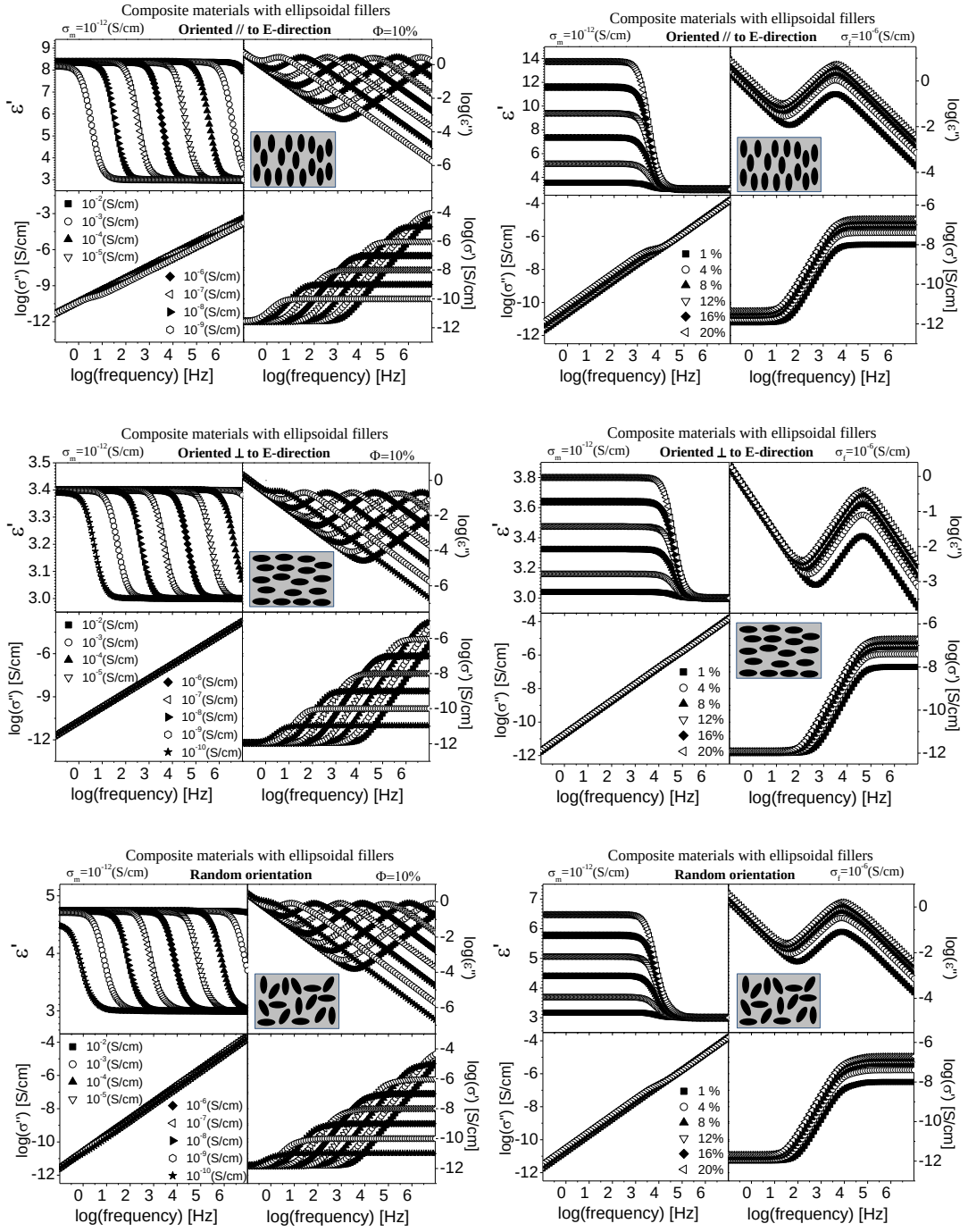
Composite materials with ellipsoidal fillers
σm=10-12(S/cm) Oriented // to E-direction Φ=10%
Composite materials with ellipsoidal fillers
σm=10-12(S/cm) Oriented // to E-direction σf=10-6(S/cm)
Composite materials with ellipsoidal fillers
σm=10-12(S/cm) Oriented ⊥ to E-direction Φ=10%
Composite materials with ellipsoidal fillers
σm=10-12(S/cm) Oriented ⊥ to E-direction σf=10-6(S/cm)
Composite materials with ellipsoidal fillers
σm=10-12(S/cm) Random orientation Φ=10%
Composite materials with ellipsoidal fillers
σm=10-12(S/cm) Random orientation σf=10-6(S/cm)
ε'
log(ε")
log(σ") [S/cm]
log(σ') [S/cm]
log(frequency) [Hz]
10-2(S/cm)
10-3(S/cm)
10-4(S/cm)
10-5(S/cm)
10-6(S/cm)
10-7(S/cm)
10-8(S/cm)
10-9(S/cm)
10-10(S/cm)
1 %
4 %
8 %
12%
16%
20%

Figure 11

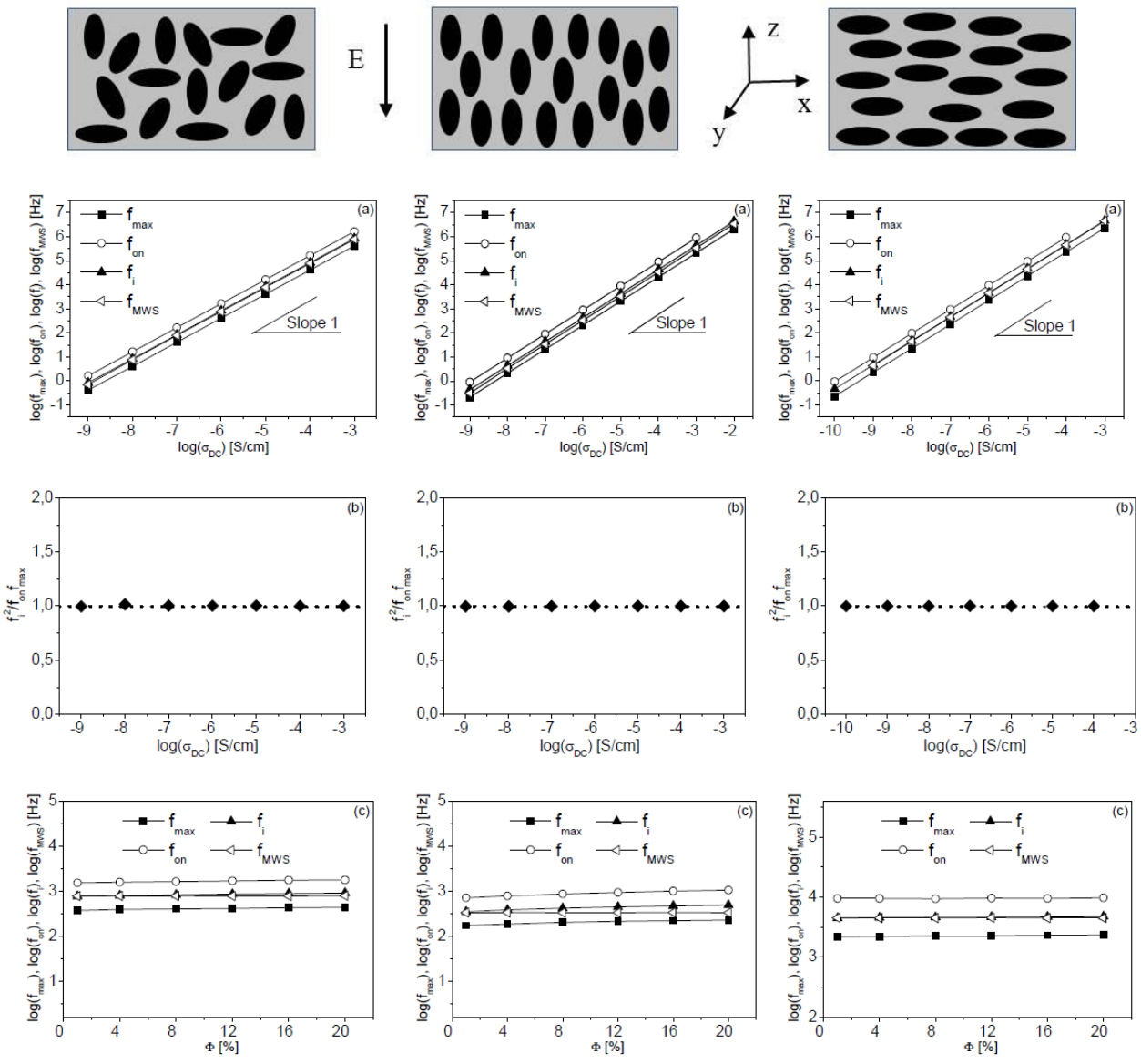

Figure 12

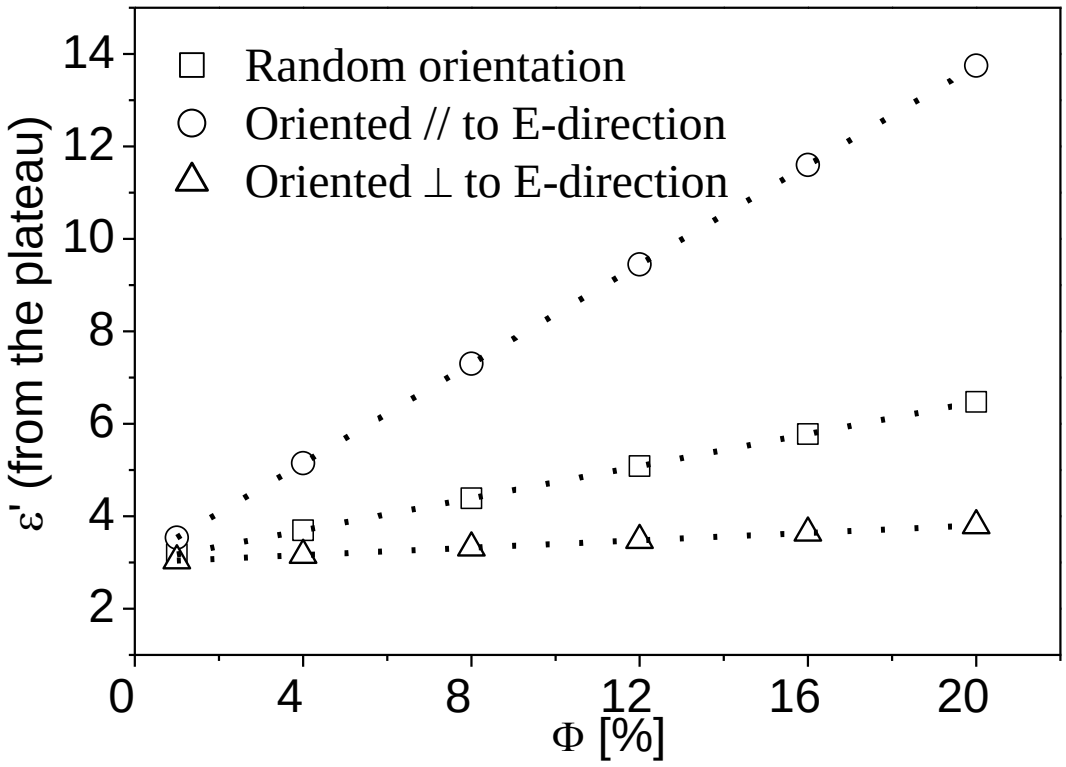
Random orientation
Oriented // to E-direction
Oriented ⊥ to E-direction
ε' (from the plateau)
Φ [%]
0
4
8
12
16
20
2
4
6
8
10
12
14

Figure 13

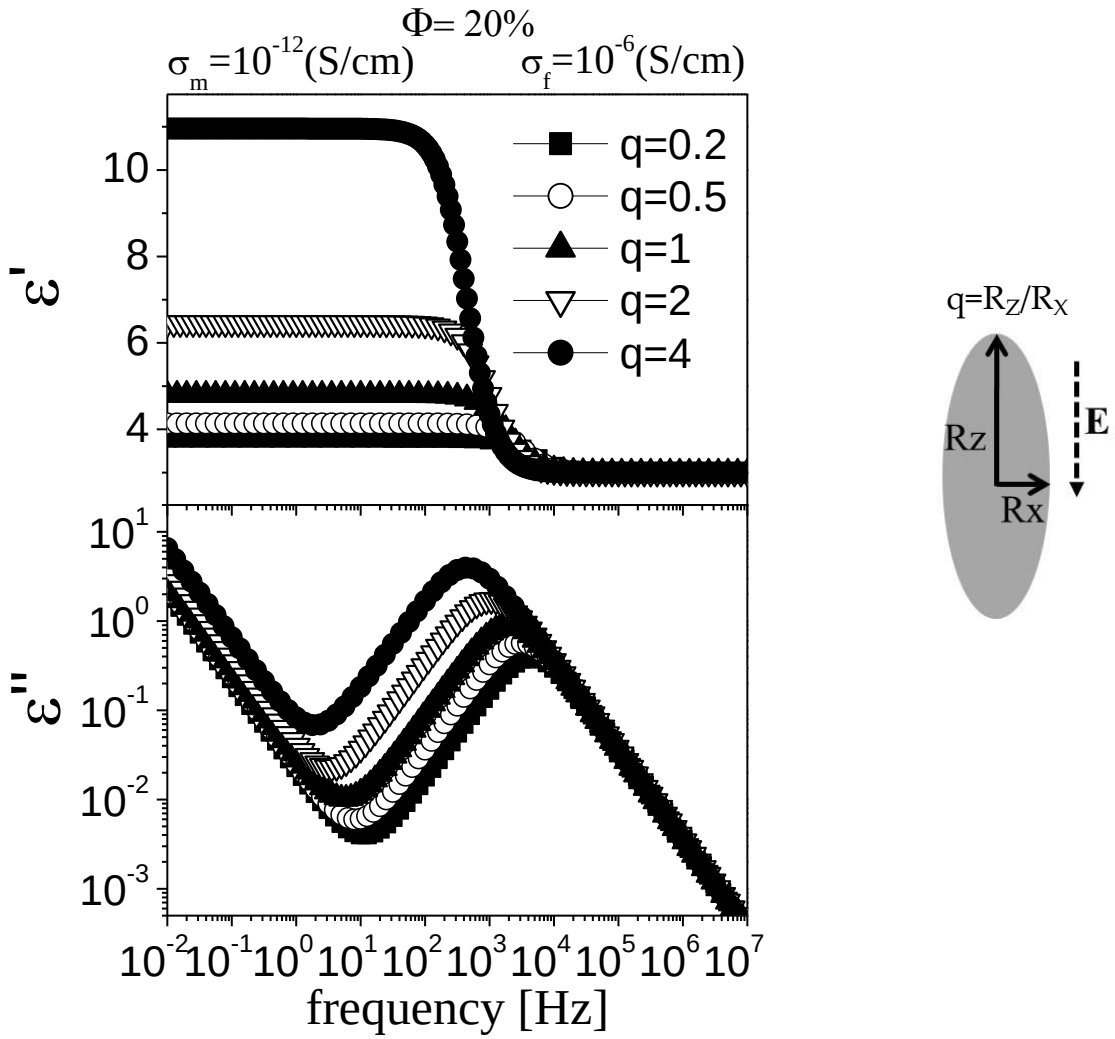
Φ= 20%
σm=10-12(S/cm)
σf=10-6(S/cm)
q=0.2
q=0.5
q=1
q=2
q=4
ε'
ε''
frequency [Hz]
q=RZ/RX
RZ
RX
E

Figure 14

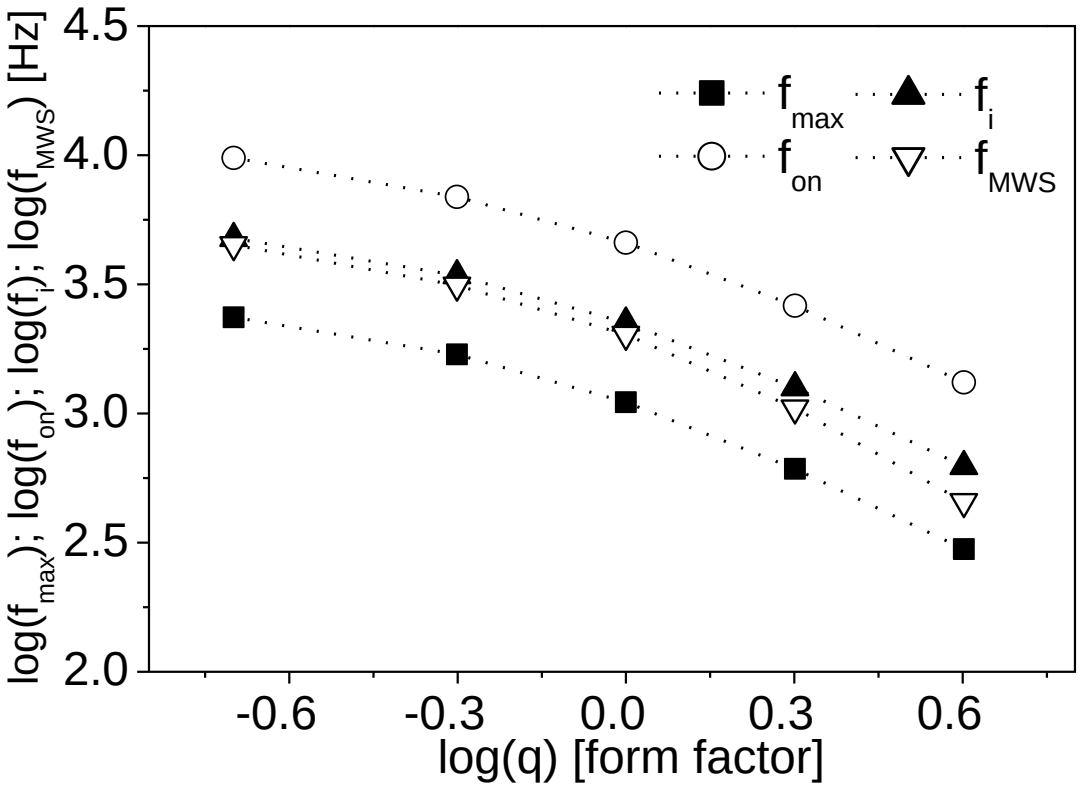
4.5
4.0
3.5
3.0
2.5
2.0
-0.6
-0.3
0.0
0.3
0.6
log(q) [form factor]
log(f_max); log(f_on); log(f_i); log(f_MWS) [Hz]
f_max
f_i
f_on
f_MWS

Figure 15

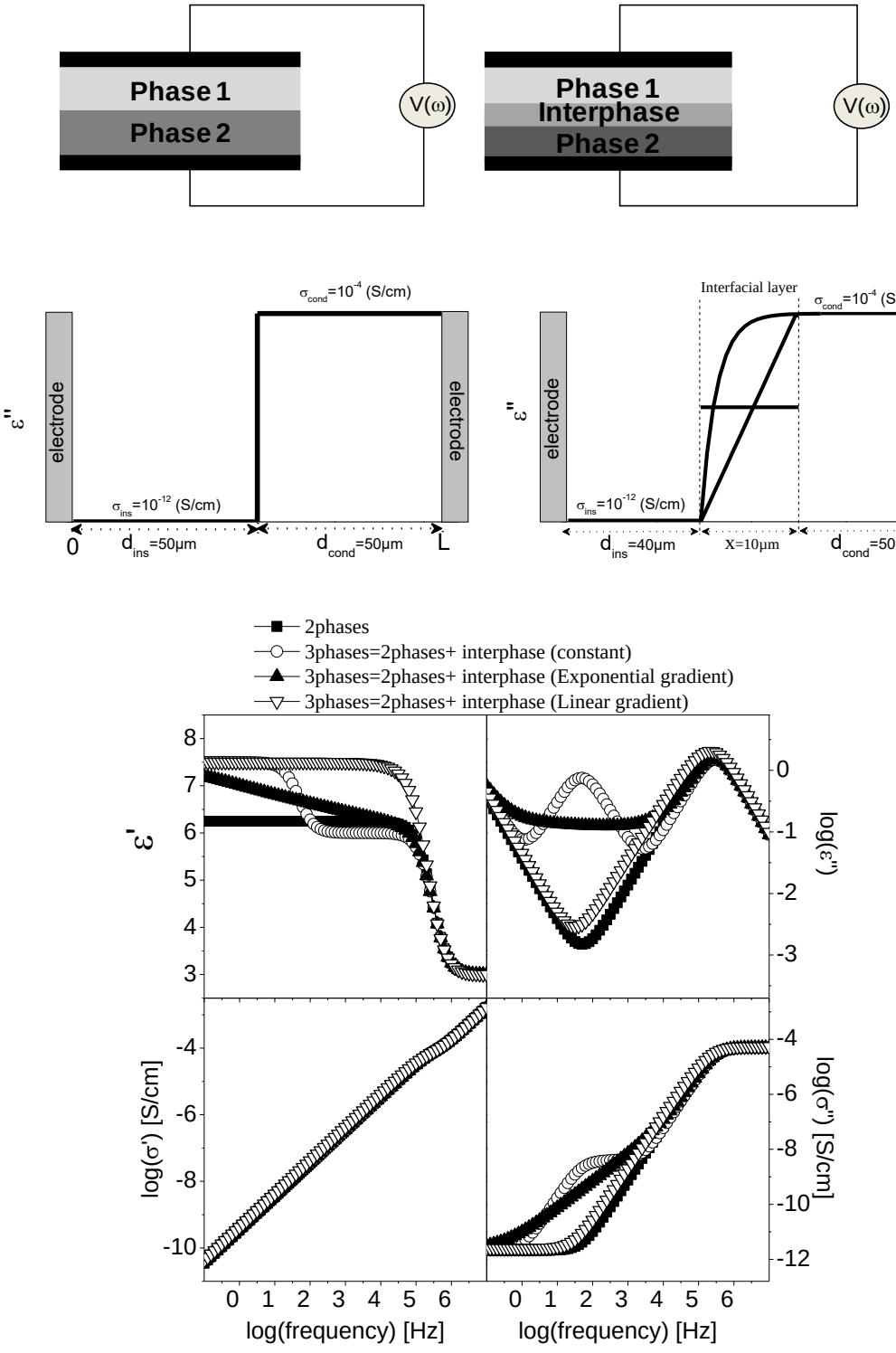
Phase 1
Phase 2
V(ω)
Phase 1
Interphase
Phase 2
V(ω)
ε"
electrode
σcond=10-4 (S/cm)
electrode
σins=10-12 (S/cm)
0
dins=50µm
dcond=50µm
L
ε"
electrode
Interfacial layer
σcond=10-4 (S/cm)
electrode
σins=10-12 (S/cm)
dins=40µm
X=10µm
dcond=50µm
2phases
3phases=2phases+ interphase (constant)
3phases=2phases+ interphase (Exponential gradient)
3phases=2phases+ interphase (Linear gradient)
ε'
log(ε")
log(σ') [S/cm]
log(σ") [S/cm]
log(frequency) [Hz]
log(frequency) [Hz]

Figure 16

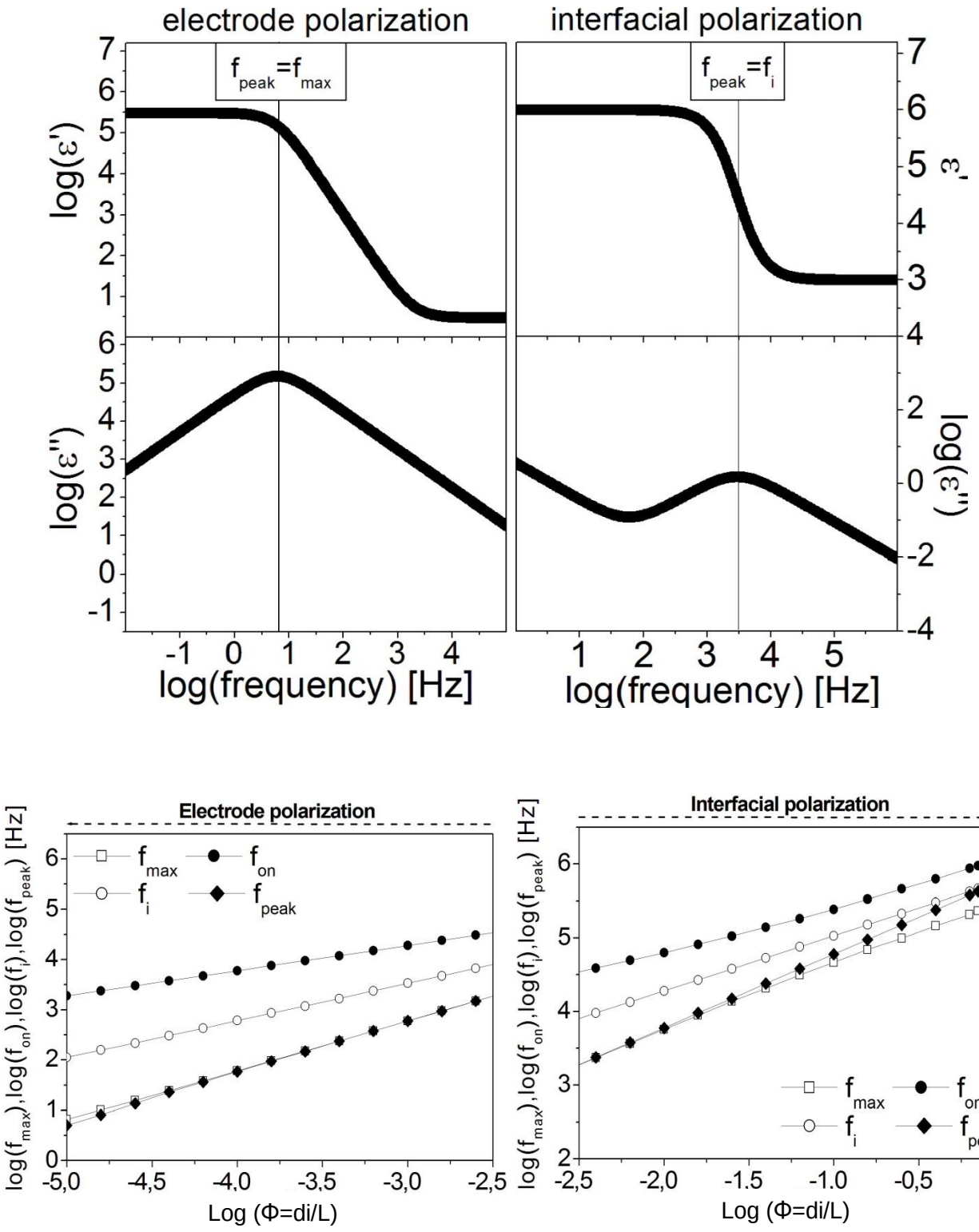
electrode polarization
interfacial polarization
f_peak=f_max
f_peak=f_i
log(ε')
log(ε'')
log(frequency) [Hz]
log(frequency) [Hz]
Electrode polarization
Interfacial polarization
log(f_max),log(f_on),log(f_i),log(f_peak) [Hz]
f_max
f_on
f_i
f_peak
Log (Φ=di/L)
Log (Φ=di/L)

Figure 17

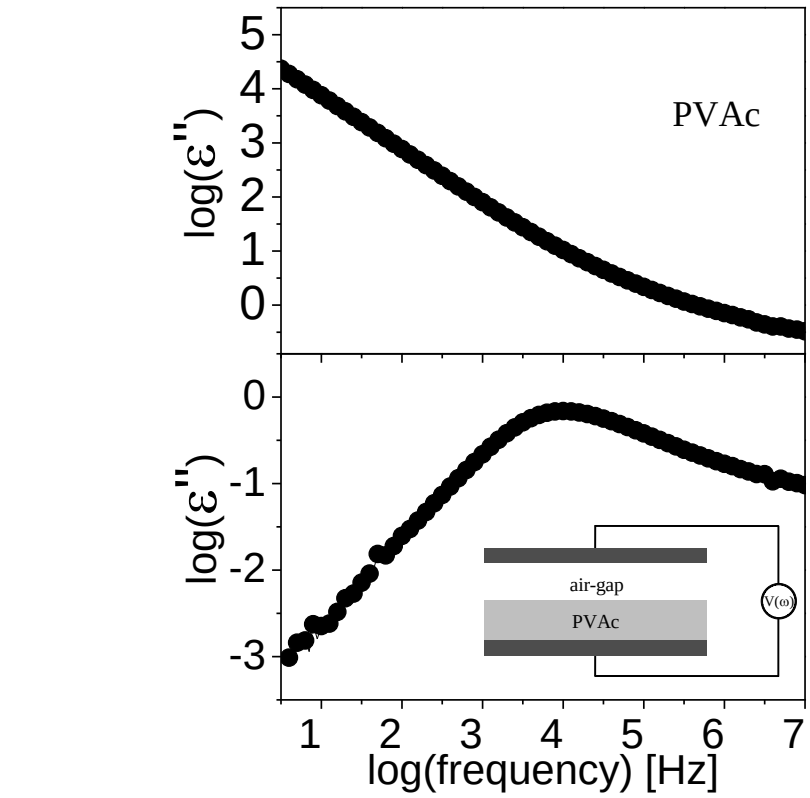
PVAc
log(ε'')
log(ε'')
air-gap
PVAc
V(ω)
log(frequency) [Hz]

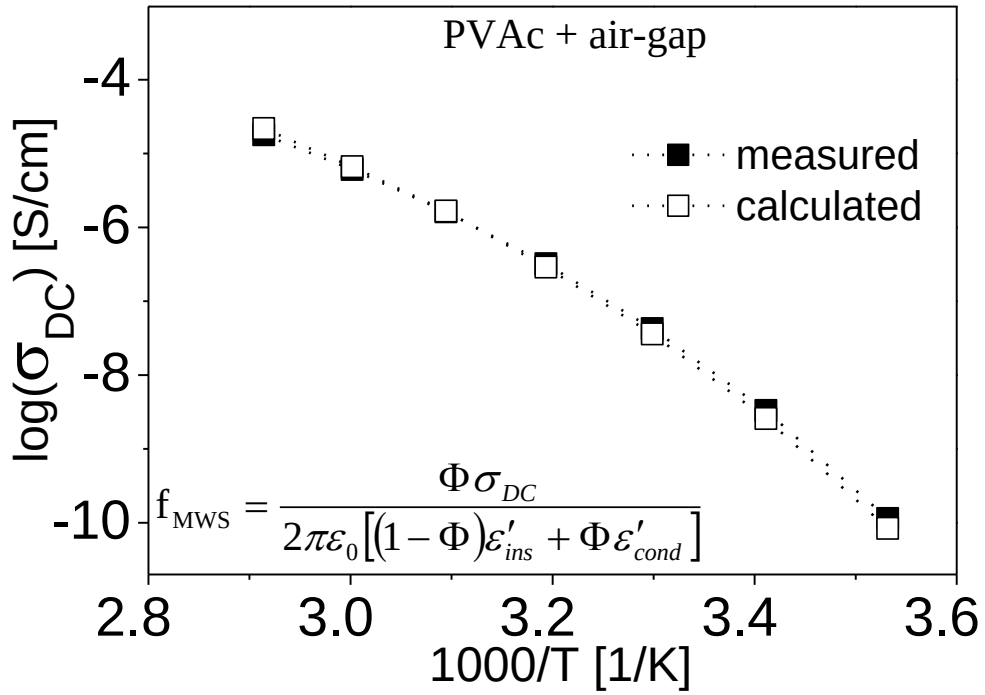
PVAc + air-gap
measured
calculated
log(σDC) [S/cm]
fMWS = ΦσDC / 2πε0[(1−Φ)ε'ins + Φε'cond]
1000/T [1/K]

Figure 18

Supplementary Material:

1- The phenomenon of interfacial polarization: basic principle

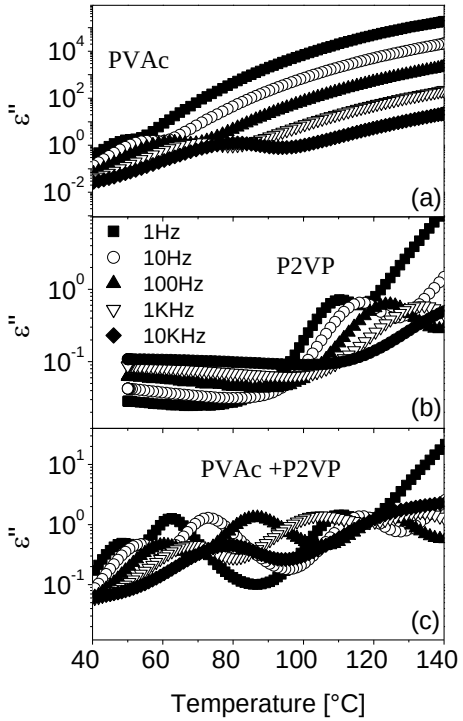

Figure S1: The dielectric loss ε'' of PVAc with a thickness of 100μm and of P2VP with 100μm in thickness, for the two samples measured separately **(a, b)** and together **(c)**, as function of temperature and at different frequencies, as indicated.

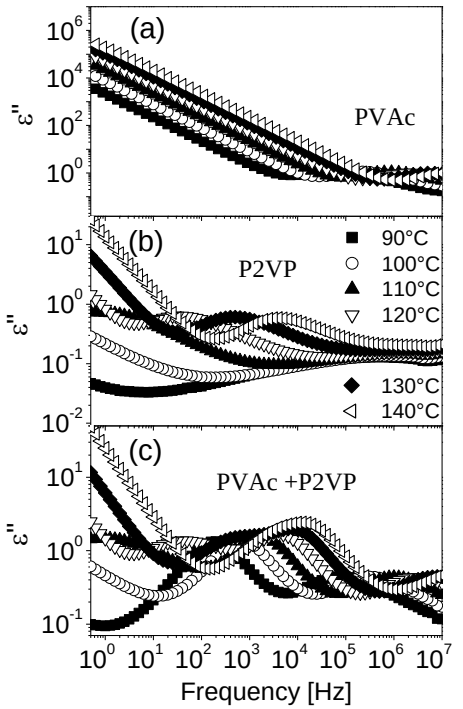

Figure S2: The dielectric loss ε'' of PVAc with a thickness of 100μm and of P2VP with 100μm in thickness, for the two samples measured separately **(a, b)** and together **(c)**, as function of frequency and at different temperature, as indicated.

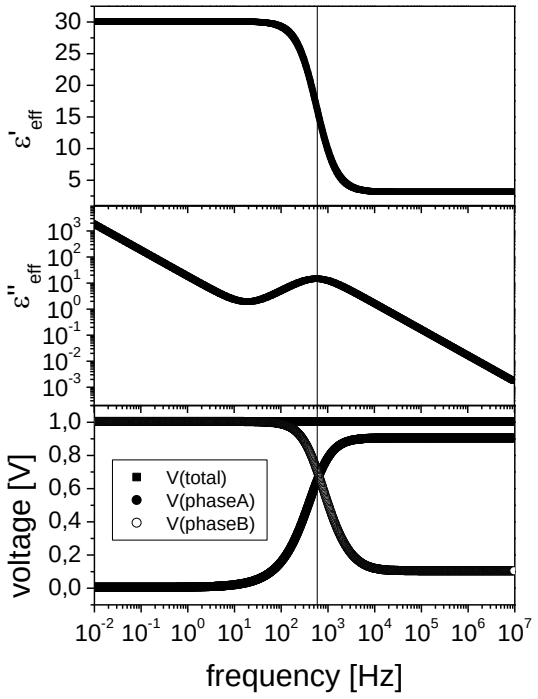

Figure S3: the effective permittivity, the effective dielectric loss and the voltage distribution of a bi-layer system consisting of two layers of different dielectric phases (phase A and phase B) having identical permittivity values ($\varepsilon_A = \varepsilon_B = 3$).The thickness values are: $d_A = 0.09mm$ for the phase A and $d_B = 0.01mm$ for the phase B. The two phase show a difference of 3 orders of magnitude between their dielectric losses, originating from a contrast of conductivity (conductivity of phase A: $\sigma_A=10^{-8}$ S/cm, conductivity of phase B: $\sigma_B=10^{-12}$ S/cm).

2- Maxwell-Wager-Sillars interfacial polarization in the electrical and dielectric behavior of multiphase materials

This study offers a complete theoretical description of the electrical and dielectric properties of multiphase materials with different morphologies.

I. Lamellar:

The dielectric properties of bi-layers structure consisting of a conductive and an insulating layer are investigated:

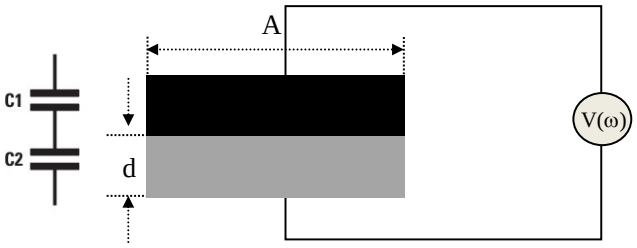

Figure S4: Bi-layers structure

According to this morphology, we have capacitance in series so we use the following expressions:

$$\frac{1}{C^*_{net}} = \frac{1}{C^*_1} + \frac{1}{C^*_2} \qquad \text{(eq.S1)}$$

With:

$$C^*_{net} = \varepsilon_0 \varepsilon^*_{net} \frac{A}{L}, C^*_1 = \varepsilon_0 \varepsilon^*_1 \frac{A}{d_1} \text{ and } C^*_2 = \varepsilon_0 \varepsilon^*_2 \frac{A}{d_2}$$

The global dielectric response can be calculated by considering the complex permittivity functions (or the complex conductivity functions) of the two phases and their corresponding thicknesses:

$$\varepsilon^*_{net} = \frac{L \varepsilon^*_{cond} \varepsilon^*_{ins}}{d_{ins} \varepsilon^*_{cond} + d_{cond} \varepsilon^*_{ins}} \qquad \text{(eq.S2)}$$

Where:

$\varepsilon^*_{cond} = \varepsilon'_{cond} - i\varepsilon''_{cond}$ represents the complex dielectric function of the conductive layer, d_{cond} its thickness, $\varepsilon^*_{ins} = \varepsilon'_{ins} - i\varepsilon''_{ins}$ the complex dielectric function of the insulating layer, d_{ins} its thickness, and $L = d_{ins} + d_{cond}$ represents the total thickness of the polymer sample. Between the complex permittivity function and the complex conductivity function a linear relationship exists, thus $\sigma^*_{cond} = i\omega\varepsilon_0 \varepsilon^*_{cond}$, with $\sigma'_{cond} = \omega\varepsilon_0 \varepsilon''_{cond}$ and $\sigma''_{cond} = \omega\varepsilon_0 \varepsilon'_{cond}$, and $\sigma^*_{ins} = i\omega\varepsilon_0 \varepsilon^*_{ins}$, with $\sigma'_{ins} = \omega\varepsilon_0 \varepsilon''_{ins}$ and $\sigma''_{ins} = \omega\varepsilon_0 \varepsilon'_{ins}$, with ω being the radial frequency of the applied electric field and ε_0 the vacuum permittivity.

The global dielectric response of bi-layers structures consisting of an insulating and a conductive polymer phase was simulated by numerical calculations using the formula:

$$\varepsilon^*_{net} = \frac{\varepsilon^*_{cond}\varepsilon^*_{ins}}{\Phi\varepsilon^*_{cond} + (1-\Phi)\varepsilon^*_{ins}} \qquad \text{(eq.S3)}$$

With $\Phi = d_{ins}/L$ being the volume fraction of the insulating phase.

Separating the real and the imaginary part, leads to:

$$\varepsilon'_{net} = \frac{\left[\left(\varepsilon'_{ins}\varepsilon'_{cond} - \varepsilon''_{ins}\varepsilon''_{cond}\right)\left((1-\Phi)\varepsilon'_{ins} + \Phi\varepsilon'_{cond}\right) + \left(\varepsilon''_{ins}\varepsilon'_{cond} + \varepsilon'_{ins}\varepsilon''_{cond}\right)\left((1-\Phi)\varepsilon''_{ins} + \Phi\varepsilon''_{cond}\right)\right]}{\left[(1-\Phi)\varepsilon'_{ins} + \Phi\varepsilon'_{cond}\right]^2 + \left[(1-\Phi)\varepsilon''_{ins} + \Phi\varepsilon''_{cond}\right]^2}$$

(eq.S4a)

$$\varepsilon''_{net} = \frac{\left[\left(\varepsilon''_{ins}\varepsilon'_{cond} + \varepsilon'_{ind}\varepsilon''_{cond}\right)\left((1-\Phi)\varepsilon'_{ins} + \Phi\varepsilon'_{cond}\right) - \left(\varepsilon'_{ins}\varepsilon'_{cond} - \varepsilon''_{ins}\varepsilon''_{cond}\right)\left((1-\Phi)\varepsilon''_{ins} + \Phi\varepsilon''_{cond}\right)\right]}{\left[(1-\Phi)\varepsilon'_{ins} + \Phi\varepsilon'_{cond}\right]^2 + \left[(1-\Phi)\varepsilon''_{ins} + \Phi\varepsilon''_{cond}\right]^2}$$

(eq.S4b)

For the complex conductivity function, the following expressions are derived:

$$\sigma'_{net} = (2\pi\varepsilon_0 f)\frac{\left[\left(\varepsilon'_{ins}\varepsilon'_{cond} - \varepsilon''_{ins}\varepsilon''_{cond}\right)\left((1-\Phi)\varepsilon'_{ins} + \Phi\varepsilon'_{cond}\right) + \left(\varepsilon''_{ins}\varepsilon'_{cond} + \varepsilon'_{ins}\varepsilon''_{cond}\right)\left((1-\Phi)\varepsilon''_{ins} + \Phi\varepsilon''_{cond}\right)\right]}{\left[(1-\Phi)\varepsilon'_{ins} + \Phi\varepsilon'_{cond}\right]^2 + \left[(1-\Phi)\varepsilon''_{ins} + \Phi\varepsilon''_{cond}\right]^2}$$

(eq.S5a)

$$\sigma''_{net} = (2\pi\varepsilon_0 f)\frac{\left[\left(\varepsilon''_{ins}\varepsilon'_{cond} + \varepsilon'_{ins}\varepsilon''_{cond}\right)\left((1-\Phi)\varepsilon'_{ins} + \Phi\varepsilon'_{cond}\right) - \left(\varepsilon'_{ins}\varepsilon'_{cond} - \varepsilon''_{ins}\varepsilon''_{cond}\right)\left((1-\Phi)\varepsilon''_{ins} + \Phi\varepsilon''_{cond}\right)\right]}{\left[(1-\Phi)\varepsilon'_{ins} + \Phi\varepsilon'_{cond}\right]^2 + \left[(1-\Phi)\varepsilon''_{ins} + \Phi\varepsilon''_{cond}\right]^2}$$

(eq.S5b)

II. Composite materials with spherical particles:

The composite material under investigation is consisting of a host matrix filled with spherical particles.

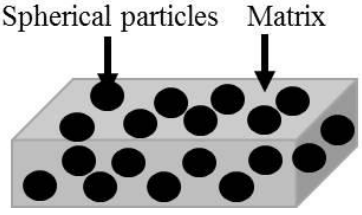

Figure S5: Composite material consisting of a host matrix embedded with spherical particles

The most general approach of calculating the net dielectric properties of composite materials consisting of a host matrix filled with spherical fillers is given by the Maxwell- Garnett equation[41-43]:

$$\varepsilon_{net}^{*}=\frac{\varepsilon_{matrix}^{*}\left[\varepsilon_{filler}^{*}\left(1+2\Phi\right)+2\varepsilon_{matrix}^{*}\left(1-\Phi\right)\right]}{\left[\varepsilon_{filler}^{*}\left(1-\Phi\right)+\varepsilon_{matrix}^{*}\left(2+\Phi\right)\right]} \qquad \text{(eq.S6)}$$

Where: Φ is the volume fraction of the fillers.

Separating the real and the imaginary part leads to:

$$\varepsilon'_{net}=\left[\left(1+\Phi\right)\left(\varepsilon'_{m}\varepsilon''_{f}-\varepsilon''_{m}\varepsilon'_{f}\right)+4\left(1-\Phi\right)\varepsilon'_{m}\varepsilon''_{m}\right]\mathrm{x}$$
$$\frac{\left[\varepsilon''_{f}\left(1-\Phi\right)+\varepsilon''_{m}\left(2+\Phi\right)\right]+\left[\left(1+2\Phi\right)\left(\varepsilon'_{m}\varepsilon'_{f}-\varepsilon''_{m}\varepsilon''_{f}\right)+2\left(1-\Phi\right)\left(\varepsilon'^{2}_{m}-\varepsilon''^{2}_{m}\right)\right]\left[\varepsilon'_{f}\left(1-\Phi\right)+\varepsilon'_{m}\left(2+\Phi\right)\right]}{\left[\varepsilon'_{f}\left(1-\Phi\right)+\varepsilon'_{m}\left(2+\Phi\right)\right]^{2}+\left[\varepsilon''_{f}\left(1-\Phi\right)+\varepsilon''_{m}\left(2+\Phi\right)\right]^{2}}$$

(eq.S7a)

And

$$\varepsilon''_{eff}=\left[\left(1+\Phi\right)\left(\varepsilon'_{m}\varepsilon''_{f}-\varepsilon''_{m}\varepsilon'_{f}\right)+4\left(1-\Phi\right)\varepsilon'_{m}\varepsilon''_{m}\right]\mathrm{x}$$
$$\frac{\left[\varepsilon'_{f}\left(1-\Phi\right)+\varepsilon'_{m}\left(2+\Phi\right)\right]-\left[\left(1+2\Phi\right)\left(\varepsilon'_{m}\varepsilon'_{f}-\varepsilon''_{m}\varepsilon''_{f}\right)+2\left(1-\Phi\right)\left(\varepsilon'^{2}_{m}-\varepsilon''^{2}_{m}\right)\right]\left[\varepsilon''_{f}\left(1-\Phi\right)+\varepsilon''_{m}\left(2+\Phi\right)\right]}{\left[\varepsilon'_{f}\left(1-\Phi\right)+\varepsilon'_{m}\left(2+\Phi\right)\right]^{2}+\left[\varepsilon''_{f}\left(1-\Phi\right)+\varepsilon''_{m}\left(2+\Phi\right)\right]^{2}}$$

(eq.S7b)

III. Composite materials with ellipsoidal particles:

The analytical formula of the global dielectric response of composite material consisting of a host matrix filled with ellipsoidal particles[44-47]:

$$\varepsilon_{net}^{*}=\varepsilon_{matrix}^{*}\left[1+\Phi\sum_{k=x,y,z}\frac{\varepsilon_{filler}^{*}-\varepsilon_{matrix}^{*}}{\varepsilon_{matrix}^{*}+\left(\varepsilon_{filler}^{*}-\varepsilon_{matrix}^{*}\right)L_{k}}\cos^{2}\varphi_{k}\right] \qquad \text{(eq.S8)}$$

Where: $\Phi=4\pi R_x R_y R_z N/3$represents the volume fraction of the ellipsoidal particles and L_k is called the depolarization factor along the k-axis, with $L_x+L_y+L_z=1$.

In this section, orientation effects are investigated:

a) Ellipsoidal particles randomly oriented:

Dielectric response of composite materials with ellipsoidal fillers randomly oriented, with $\left\langle \cos^2 \varphi_k \right\rangle = 1/3$, is given by:

$$\varepsilon^*_{net} = \varepsilon^*_{matrix}\left[1+\frac{1}{3}\Phi \sum_{k=x,y,z} \frac{\varepsilon^*_{filler}-\varepsilon^*_{matrix}}{\varepsilon^*_{matrix}+\left(\varepsilon^*_{filler}-\varepsilon^*_{matrix}\right)L_k}\right] \qquad \text{(eq.S9)}$$

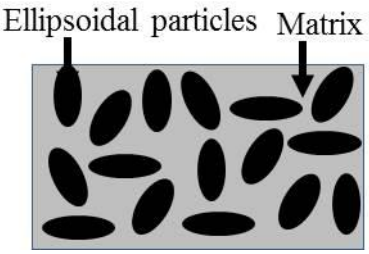

Figure S6: Structure of a dispersion of randomly oriented ellipsoidal fillers

b) Oriented ellipsoidal particles:

Composite materials with oriented ellipsoidal fillers can be analyzed, when the k-axis is parallel to E direction, the formula (S8) becomes:

$$\varepsilon^*_{net} = \varepsilon^*_{matrix}\left[1+\Phi \frac{\varepsilon^*_{filler}-\varepsilon^*_{matrix}}{\varepsilon^*_{matrix}+\left(\varepsilon^*_{filler}-\varepsilon^*_{matrix}\right)L_k}\right] \qquad \text{(eq.S10)}$$

Two orientations can be obtained; long axis of the ellipsoid can be parallel or perpendicular to the **E**-direction, as presented in the Figure S.7 below:

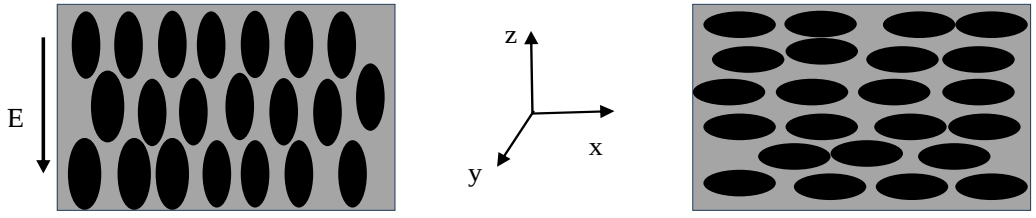

(a) (b)

Figure S7: Structure of a dispersion of oriented ellipsoidal fillers **(a)** Prolate ellipsoids: fillers oriented parallel to the **E**-direction **(b)** Oblate ellipsoids: fillers oriented perpendicular to the **E**-direction

(a) Prolate ellipsoids ($R_z > R_x$), the form factor: $q = \frac{R_z}{R_x} > 1$ and the depolarization factor has the following expression:

$$L_z = -\frac{1}{q^2-1} + \frac{q}{\left(q^2-1\right)^{3/2}} \ln\left[q + \left(q^2-1\right)^{1/2}\right] \quad \text{(eq.S11a)}$$

(b) Oblate ellipsoids ($R_z < R_x$), $q = \frac{R_z}{R_x} \langle 1$ and the depolarization factor is:

$$L_z = \frac{1}{1-q^2} + \frac{q}{\left(1-q^2\right)^{3/2}} \cos^{-1} q \quad \text{(eq.S11b)}$$

(iv) Composite materials with cylindrical fillers:

Actually, the fillers particles can be of any ellipsoidal shape. Special cases such as cylinders particles can be covered and analyzed by the analytical formula (S8) in dependence to the form factor q which is the axial ratio of the particles ($q=R_z/R_x$), thus the depolarization factor L_k.

- Cylinders perpendicular to the direction of the dielectric field:

The corresponding equation is obtained by substituting 1/2 for L_k in the equation (S11b):

$$\varepsilon^*_{net} = \varepsilon^*_m \left[1 + 2\Phi \frac{\varepsilon^*_f - \varepsilon^*_m}{\varepsilon^*_m + \varepsilon^*_f}\right] \quad \text{(eq.S12)}$$

3- Experimental data to investigate the phenomenon of interfacial MWS polarization.

a) Composite material consisting of a host matrix embedded with cylinder fillers

Dielectric properties of composite material consisting of a host matrix embedded with cylinder fillers were characterized by Broadband Dielectric Spectroscopy. The polytetraflouroethylene (PTFE) was filled with an ionic liquid (EMIM SCN, 1-Ethyl-3-methylimidazolium thiocyanate, from Iolitec), as illustrated in the Figure S8.

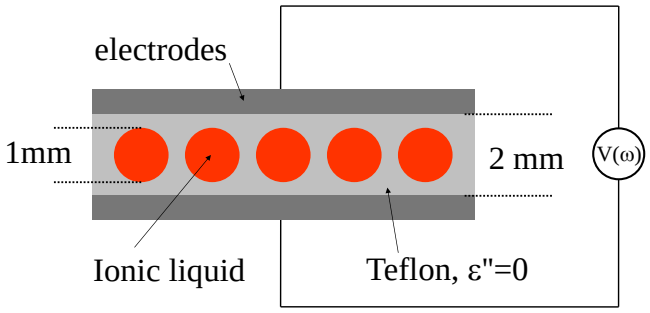

Figure S8: A host matrix embedded with cylinder fillers

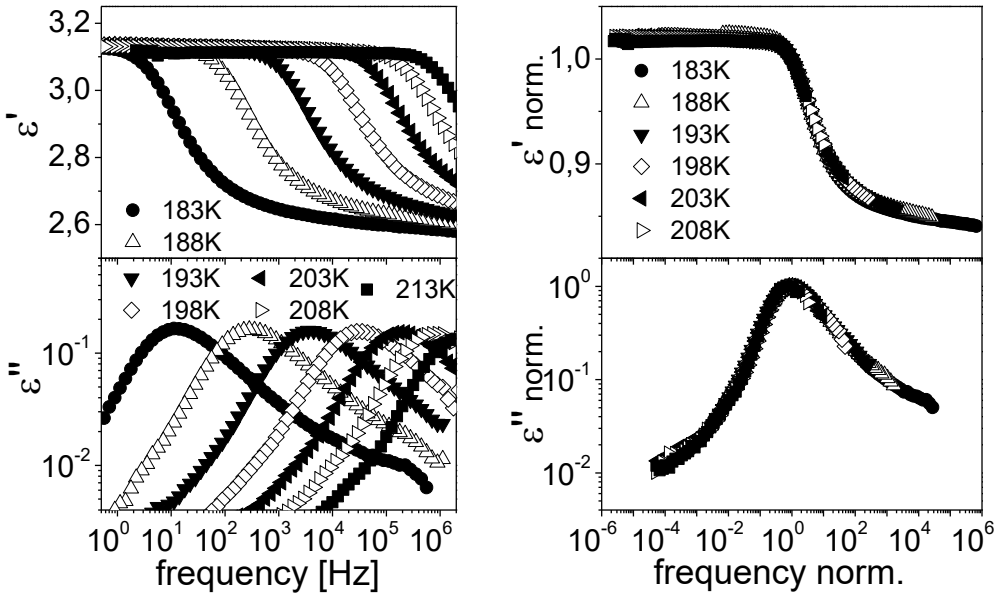

Figure S9: (left graphs) Complex permittivity measured for a composite material with cylinder fillers, as a function of frequency at different values of temperature. **(right graphs)** Normalized curves for the data presented in left graphs.

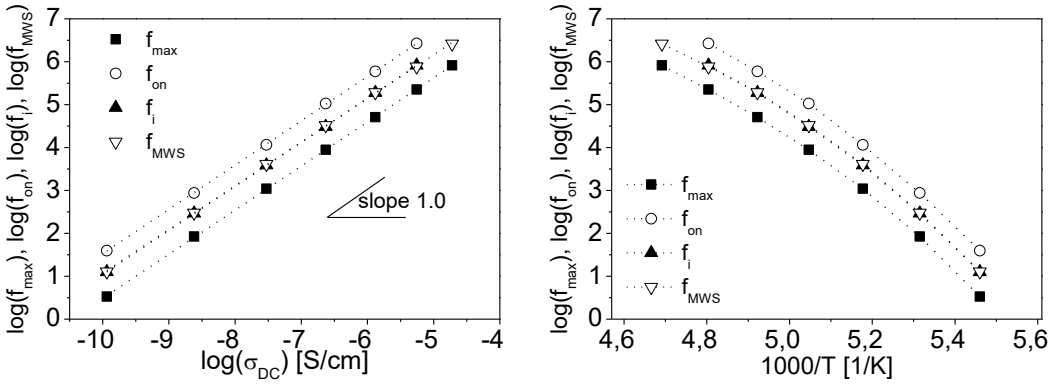

Figure S10: **(a)** The characteristic frequencies f_{max}, f_{on}, f_i and f_{MWS} (determined from the dielectric measurements presented in Fig. S9) plotted as a function of the measured DC-conductivity **(b)** as a function of the inverse of temperature.

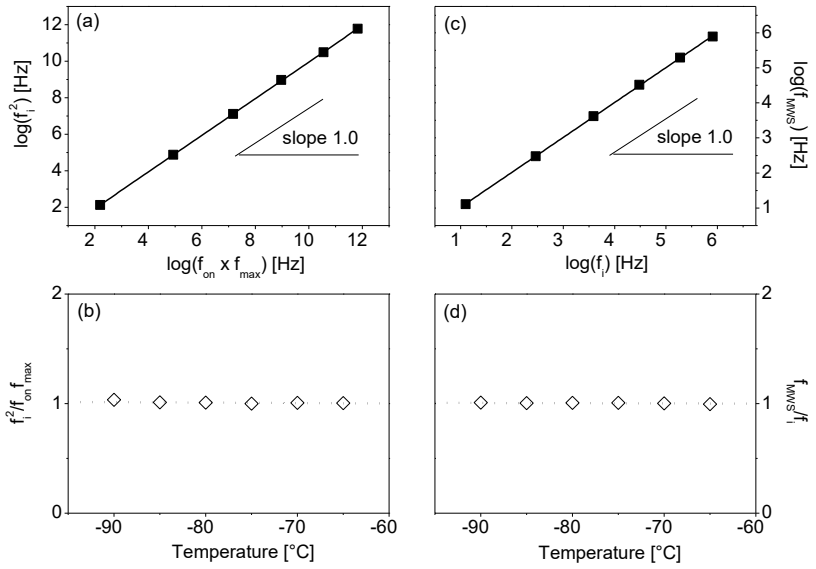

Figure S12: (a) f_i^2 vs. $f_{on}f_{max}$ for the data presented in fig.S9 (**b)** the ratio $f_i^2/(f_{on}f_{max})$ for different values of temperature. **(c)** f_{MWS} as a function of f_i. **(d)**the ratio f_{MWS}/f_i for different values of temperature

b) Bi-layers materials:

Dielectric measurements by Broadband Dielectric Spectroscopy have been carried out for bi-layer sample consisting of a conductive (PVAc_4%BMIM BF4, thickness200μm) and an isolating polymer phase (PTFE, thickness 25μm) was investigated.

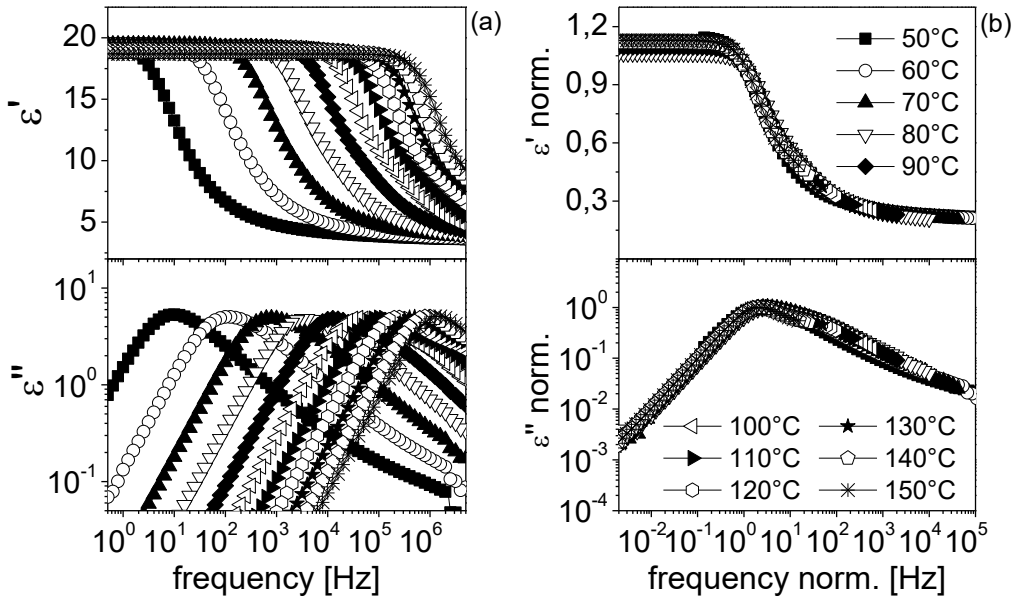

Figure S13: **(a)** Complex permittivity measured as a function of frequency at different values of temperature. **(b)** Normalized curves for the data presented in fig.13a

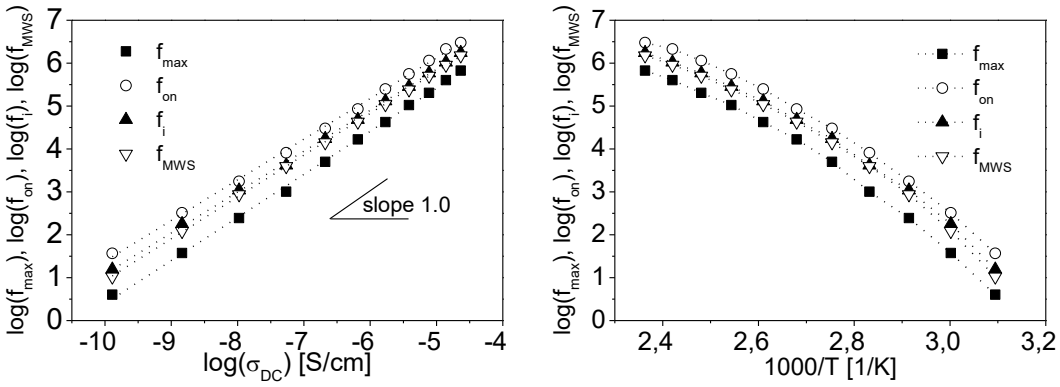

Figure S14: (left) The characteristic frequencies f_{max}, f_{on}, f_i and f_{MWS} (determined from the dielectric measurements presented in Fig. S13) plotted as a function of the measured DC-conductivity **(right)** as a function of the inverse of temperature.

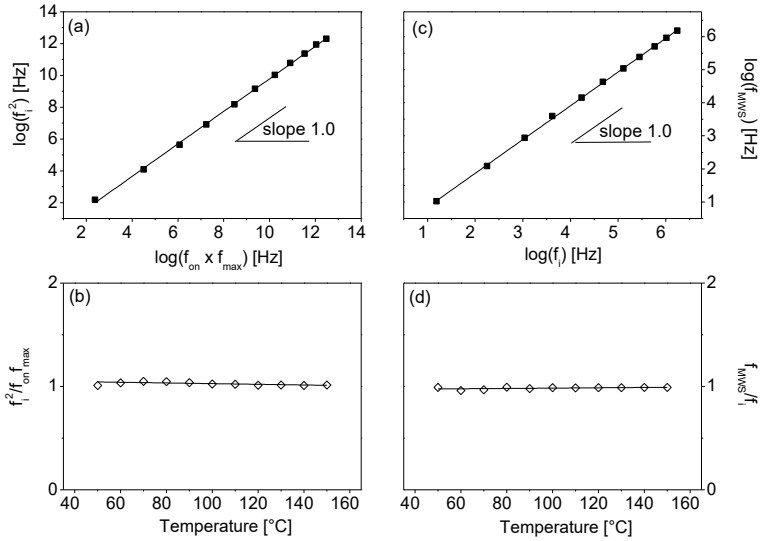

Figure S15: **(a)** f_i^2 vs. $f_{on}f_{max}$ for the data presented in fig. S13 **(b)** The ratio $f_i^2/(f_{on}f_{max})$ for different values of temperature. **(c)** f_{MWS} as a function of f_i. **(d)** The ratio f_{MWS}/f_i for different values of temperature.